Chapter II. In-Situ and Remote Sensing Measurements of Aerosol Properties, Burdens, and Radiative Forcing

Authors: H. Yu, NASA GSFC/UMBC; **P. Quinn**, NOAA PMEL; **M. Chin**, NASA GSFC; **L. Remer**, NASA GSFC; **G. Feingold**, NOAA ESRL.

Table of Contents

2.1. Introduction

Over the past decade and since the IPCC TAR in particular, a great deal of effort has gone into improving measurement data sets (as summarized in Yu et al., 2006; Bates et al., 2006; Kahn et al., 2004a), including

- Execution of intensive field experiments examining aerosol processes and properties in various aerosol regimes around the globe;
- Establishment and enhancement of ground-based networks measuring aerosol properties and radiative effects;
- Development and deployment of new and enhanced instrumentation, importantly aerosol mass spectrometers examining size dependent composition, and;
- Development and implementation of new and enhanced satellite-borne sensors examining aerosol effects on atmospheric radiation.

These dedicated efforts make it feasible to shift the estimates of aerosol radiative effect and climate forcing from largely model-based as in IPCC TAR to increasingly measurement-based as in the IPCC Fourth Assessment Report (AR4) (IPCC 2007). Satellite measurements that are evaluated, supplemented, and constrained by ground-based remote sensing measurements and in-situ measurements from intensive field campaigns, provide the basis for the regional- to global-scale assessments. Chemical transport models (CTMs) are used to interpolate and supplement the data in regions/conditions where observational data are not available or to assimilate data from various observations for constraining and thereby improving model simulations of aerosol impacts. These developments have played an important role in advancing the scientific understanding of aerosol direct and indirect forcing as documented in the IPCC AR4 (Forster et al., 2007).

In this chapter we review the capabilities of aerosol measurements developed over the past decade, describe the synergies between different measurements and models, and discuss outstanding issues.

2.2. Overview of Aerosol Measurement Capabilities

2.2.1. *Intensive Field Campaigns*

Over the past two decades, more than a dozen intensive field experiments have been conducted to study the physical, chemical, and optical properties and radiative effects of aerosols in a variety of aerosol regimes around the world, as listed in **Table 2.1.** These experiments have been designed with aerosol characterization as the main goal or as one of the major themes in more interdisciplinary studies.

Several of these experiments have been designed to characterize regional aerosol properties in marine environments downwind of known continental aerosol source regions, including:

- The first Aerosol Characterization Experiment (ACE 1) which took place in the Southern Ocean environment south of Australia to characterize background, clean marine aerosol upon which anthropogenic forcings could be imposed (Bates et al., 1998)

Table 2.1: List of major intensive field experiments that are relevant to aerosol research in a variety of aerosol regimes around the globe conducted in the past two decades (adapted from Yu et al., 2006).

Aerosol Regimes	Intensive Field Experiments			Major References
	Name	Location	Time	
Industrial Pollution from North America and West Europe	TARFOX	North Atlantic	July, 1996	Russell et al., 1999
	NEAQS	North Atlantic	July – August, 2002	Quinn and Bates, 2003
	SCAR-A	North America	1993	Remer et al., 1997
	CLAMS	East Coast of U.S.	July-August, 2001	Smith et al., 2005
	INTEX-NA, ICARTT	North America	Summer 2004	Fehsenfeld et al., 2006
	ACE-2	North Atlantic	June – July, 1997	Raes et al., 2000
	MINOS	Mediterranean region	July - August, 2001	Lelieveld et al., 2002
	LACE98	Lindberg, Germany	July-August, 1998	Ansmann et al., 2002
	Aerosols99	Atlantic	January - February, 1999	Bates et al., 2001
Brown Haze in South Asia	INDOEX	Indian subcontinent and Indian Ocean	January - April, 1998 and 1999	Ramanathan et al., 2001b
	ABC	South and East Asia	ongoing	Ramanathan and Crutzen, 2003
Pollution and dust mixture in East Asia	EAST-AIRE	China	March-April, 2005	Li et al., 2007
	ACE-Asia	East Asia and Northwest Pacific	April, 2001	Huebert et al., 2003; Seinfeld et al., 2004
	TRACE-P		March - April, 2001	Jacob et al., 2003
	PEM-West A & B	Western Pacific off East Asia	September-October, 1991 February-March, 1994	Hoell et al., 1996; 1997
Biomass burning smoke in the tropics	BASE-A	Brazil	1989	Kaufman et al., 1992
	SCAR-B	Brazil	August - September, 1995	Kaufman et al., 1998
	LBA-SMOCC	Amazon basin	September-November 2002	Andreae et al., 2004
	SAFARI2000	South Africa and South Atlantic	August - September, 2000	King et al., 2003a
	SAFARI92		September – October, 1992	Lindesay et al., 1996
	TRACE-A	South Atlantic	September-October, 1992	Fishman et al., 1996
Mineral dusts from North Africa and Arabian Peninsula	SHADE	West coast of North Africa	September, 2000	Tanré et al., 2003
	PRIDE	Puerto Rico	June – July, 2000	Reid et al., 2003
	UAE[2]	Arabian Peninsula	August - September, 2004	Reid et al., 2008
Remote Oceanic Aerosol	ACE-1	Southern Oceans	December, 1995	Bates et al., 1998; Quinn and Coffman, 1998

Table 2.2: Summary of major surface networks for the tropospheric aerosol characterization and climate forcing research.

Surface Network	Measured/derived parameters				Spatial coverage	Temporal coverage
	Loading	Size, shape	Absorption	Chemistry		
NASA AERONET	optical depth	fine-mode fraction, Angstrom exponents, asymmetry factor, phase function, non-spherical fraction	single-scattering albedo, absorption optical depth, refractive indices	N/A	~200 sites over global land and islands	1993 onward
DOE ARM					6 sites and 4 mobile facilities in North America, Europe, and Asia	1989 onward
NOAA GMD	near-surface extinction coefficient, optical depth, CN/CCN number concentrations	Angstrom exponent, upscatter fraction, asymmetry factor, hygroscopic growth	single-scattering albedo, absorption coefficient	chemical composition in selected sites and periods	4 baseline stations, several regional stations, aircraft and mobile platforms	1976 onward
AERONET-MAN	optical depth	N/A	N/A	N/A	global ocean	2004-present (periodically)
NASA MPL	vertical distributions of backscatter/extinction coefficient, optical depth	N/A	N/A	N/A	~30 sites in major continents, usually collocated with AERONET and ARM sites and major field experiments	2000 onward
IMPROVE	near-surface mass concentrations and extinction coefficients by species	fine and coarse separately	single-scattering albedo, absorption coefficient	ions, ammonium sulfate, ammonium nitrate, organics, elemental carbon, fine soil	156 national parks and wilderness areas in the U.S.	1988 onward

- The second Aerosol Characterization Experiment (ACE 2) which took place in the subtropical northeast Atlantic Ocean and focused on the European aerosol plume (Raes et al., 2000).
- The Indian Ocean Experiment (INDOEX) which characterized the plumes emanating from the Indian subcontinent and nearby regions as they were transported out over the Indian Ocean (Ramanathan et al., 2001).
- The Asia Aerosol Characterization Experiment (ACE-Asia) which focused on the plume downwind of Asia (Huebert et al., 2003) as did the Transport and Chemical Evolution over the Pacific (TRACE-P) experiment (Jacob et al., 2003).
- The International Consortium for Atmospheric Research on Transport and Transformation (ICARTT) experiment, Tropospheric Aerosol Radiative Forcing Observational Experiment (TARFOX) and several other experiments that focused on the eastern U.S. plume (Fehsenfeld et al., 2006; Russell et al., 1999; Quinn and Bates, 2003).
- The South African Regional Science Initiative (SAFARI) experiment which investigated how the biomass burning smoke from South Africa influences atmospheric chemistry, the radiation budget, and climate (King et al., 2003).
- The SaHAran Dust Experiment (SHADE), Puerto Rico Dust Experiment (PRIDE), and the United Arab Emirates Unified Aerosol Experiment (UAE2) which focused on dust plumes from North Africa and the Arabian Peninsula (Tanré et al., 2003; Reid et al., 2003).

- The DOE Aerosol Intensive Operating Period (AIOP) field studies under the Atmospheric Radiation Measurement (ARM) program that targeted at characterizing aerosol optical properties and radiative influence (Ferrare et al., 2006).
- Field studies that examine aerosol formation and near source evolution in urban regions (Solomon et al., 2003; Zhang et al., 2004; Salcedo et al., 2006).

During each of these comprehensive experiments, aerosols were studied in great detail, using combinations of in-situ and remote sensing observations of physical and chemical properties from various platforms (e.g., aircraft, ship, satellite, and ground-based networks) and numerical modeling. In spite of their relatively short duration, these field experiments have acquired comprehensive data sets of regional aerosol properties that can be compared and compiled to understand the complex interactions of aerosols within the earth and atmosphere system.

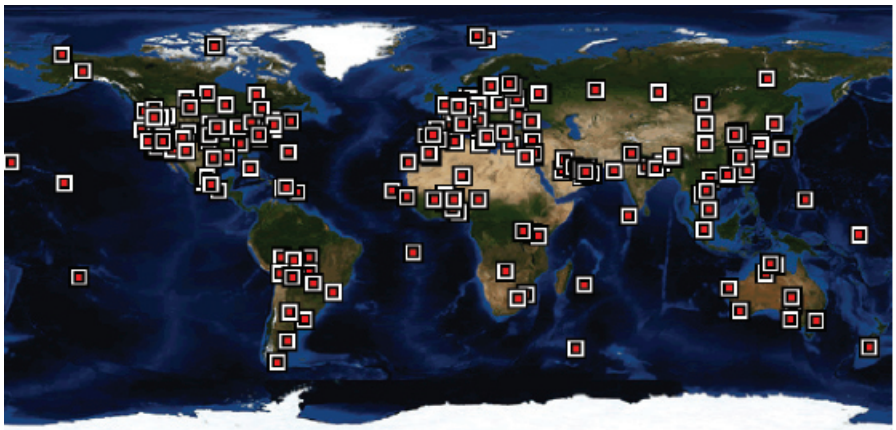

Figure 2.1: Geographical coverage of active AERONET sites in 2006.

2.2.2. *Ground-based Remote Sensing and In-Situ Measurement Networks*

Major surface networks for the tropospheric aerosol characterization and climate forcing research are listed in **Table 2.2**.

2.2.2.1. *Ground-based remote sensing.*

The Aerosol Robotic Network (*AERONET*) program is a federated ground-based remote sensing network of well-calibrated sun photometers and radiometers (http://aeronet.gsfc.nasa.gov). AERONET includes about 200 sites around the world, covering all major tropospheric aerosol regimes (Holben et al., 1998; 2001), as illustrated in **Figure 2.1**. Spectral measurements of sun and sky radiance are calibrated and screened for cloud-free conditions (Smirnov et al., 2000). AERONET stations provide:

- direct, calibrated measurements of spectral aerosol optical depth (AOD or τ) (normally at wavelengths of 440, 670, 870, and 1020 nm) with an accuracy of ±0.015 (Eck et al. 1999), and
- inversion-based retrievals of a variety of effective, column-mean properties, including aerosol single-scattering albedo (*SSA or* ω_0), size distributions, fine-mode fraction, the degree of nonsphericity, phase function, and asymmetry factor (Dubovik et al., 2000; Dubovik and King, 2001; Dubovik et al., 2002; O'Neill, et al., 2004). These retrieved parameters are systematically validated by comparison to emerging in-situ measurements with improved accuracy (e.g., Haywood et al., 2003; Magi et al., 2005; Leahy et al., 2007).

Recent developments associated with AERONET algorithms and data products include:

- simultaneous retrieval of aerosol and surface properties using combined AERONET and satellite measurements (Sinyuk et al., 2007);
- the addition of ocean color and high frequency solar flux measurements;
- the establishment of the Maritime Aerosol Network (MAN) component to monitor aerosols over the World oceans (Smirnov et al., 2006); and
- the extension of observations of cloud optical properties and cloud cover (Marshak et al., 2004; Kaufman and Koren, 2006).

Because of consistent calibration, cloud-screening, and retrieval methods, uniform data are available for all stations, some of which have operated for over 10 years. These data constitute a high-quality, ground-based aerosol climatology and, as such, have been widely used for aerosol process studies as well as for evaluation and validation of model simulation and satellite remote sensing applications (e.g., Chin et al., 2002; Yu et al., 2003, 2006; Remer et al., 2005; Kahn et al., 2005a). In addition, AERONET retrievals of aerosol size distribution and refractive indices have been used in algorithm development for satellite sensors (Remer et al., 2005; Levy et al., 2007a).

AERONET measurements have been complemented by other ground-based aerosol networks with less geographical or temporal coverage, such as the Atmospheric Radiation Measurement (ARM) network (Ackerman and Stokes, 2003) and other networks with multifilter rotating shadowband radiometer (*MFRSR*) (Harrison et al., 1994; Michalsky et al., 2001), the NOAA Global Monitoring Division (*GMD*) network (e.g., Delene and Ogren, 2002; Sheridan and Ogren, 1999), the Interagency Monitoring of Protected Visual Environment (*IMPROVE*) (Malm et al., 1994), and several lidar networks including

- NASA Micro Pulse Lidar Network (MPLNET) (Welton et al., 2001; 2002);
- Regional East Atmospheric Lidar Mesonet (REALM) in North America (Hoff et al., 2002; 2004);
- European Aerosol Research Lidar Network (EARLINET) (Matthias et al., 2004); and
- Asian Dust Network (AD-Net) (e.g., Murayama et al., 2001).
- The aerosol extinction profiles derived from these lidar networks with state-of-the-art techniques (Schmid et al., 2006) are pivotal to a better assessment of aerosol climate forcing and atmospheric responses.

2.2.2.2. *In-situ measurement networks*.

Long-term in-situ measurements of aerosol optical properties and chemical composition have been made in several of the regions where recent intensive field campaigns have been conducted. These measurements are part of the NOAA GMD aerosol monitoring program (Delene and Ogren, 2002; Sheridan and Ogren, 1999; Quinn et al., 2000). The measurement protocols are similar to those used during the intensive campaigns and the measurement periods often encompass the intensive campaign time periods. Hence, they provide a longer-term measure of the means and variability of aerosol properties and context for the shorter duration measurements of the intensive field campaigns.

2.2.3. *Satellite Remote Sensing*

A measurement-based characterization of aerosols on a global scale can only be realized through satellite remote sensing, due to the large spatial and temporal heterogeneities of aerosol distributions. Monitoring aerosols from space has been performed for over two decades and is planned for the coming decade with enhanced capabilities (King et al., 1999; Foster et al., 2007; Lee et al., 2006; Mishchenko et al., 2007a). **Table 2.3** summarizes major satellite measurements currently available for the tropospheric aerosol characterization and climate forcing research.

Early aerosol monitoring from space relied on sensors that were designed for other purposes. The Advanced Very High Resolution Radiometer (*AVHRR*), intended as a weather satellite, provides radiance observations in the visible and near infrared wavelengths that are sensitive to aerosol properties over the ocean (Husar et al., 1997; Mishchenko et al., 1999). Originally intended for ozone monitoring, the ultraviolet channels used for the Total Ozone Mapping Spectrometer (*TOMS*) are sensitive to aerosol absorption with little surface interferences, even over land (Torres et al., 1998). TOMS has proved to be extremely successful in monitoring biomass burning smoke and dust (Herman et al., 1997) and retrieving aerosol single-scattering albedo from space (Torres et al., 2005). A new sensor, the Ozone Monitoring Instrument (*OMI*) aboard Aura, has improved on such advantages. Such historical sensors have provided multi-decadal climatology of aerosol optical depth that has significantly advanced the understanding of aerosol distributions and long-term variability (e.g., Geogdzhayev et al., 2002; Torres et al., 2002; Massie et al., 2004; Mishchenko et al., 2007b).

Over the past decade, satellite aerosol retrievals have become increasingly sophisticated. Now, satellites measure the angular dependence of polarization and radiance in multiple wavelengths in the ultraviolet (UV) through the infrared (IR) at fine temporal and spatial resolution. From these observations, retrieved aerosol products include not only optical depth at one wavelength, but spectral optical depth and particle size over both ocean and land, as well as more direct measurements of polarization and phase function. In addition, cloud screening is much more robust than before and onboard calibration is now widely available. Examples of such new and enhanced sensors include MODerate resolution Imaging Spectroradiometer (*MODIS*, see **Box 2.1**), Multi-angle Imaging SpectroRadiometer (*MISR*, see **Box 2.2**), Polarization and Directionality of the Earth's Reflectance (*POLDER*), OMI, among others. The Clouds and the Earth's Energy System (*CERES*, see **Box 2.3**) measures broadband solar and terrestrial radiances. These radiation measurements in combination with satellite retrievals of aerosol can be used to deduce observational-based aerosol direct effect and forcing.

Complementary to these passive sensors, active remote sensing from space is also making promising progress (see **Box 2.4**). Both the Geoscience Laser Altimeter System (*GLAS*) and the Cloud and Aerosol Lidar with Orthogonal Polarization (*CALIOP*) are collecting essential information about aerosol vertical distributions. Furthermore, the constellation of six afternoon-overpass spacecrafts (as illustrated in **Figure 2.2**), so-called *A-Train* (Stephens et al., 2002) makes it possible for the first time to conduct near simultaneous (within 15-minutes) measurements of aerosols, clouds, and radiative fluxes in multiple dimensions with sensors with complementary capabilities.

Table 2.3: Summary of major satellite measurements currently available for the tropospheric aerosol characterization and climate forcing research.

Category	Properties	Sensor/platform	Parameters	Spatial coverage	Temporal coverage
Column-integrated	Loading	AVHRR/NOAA-series	optical depth	global ocean	1981-present
		TOMS/Nimbus, ADEOS1, EP		global land+ocean	1979-2001
		POLDER-1, -2, PARASOL			1997-present
		MODIS/Terra, Aqua			2000-present (Terra) 2002-present (Aqua)
		MISR/Terra			2000-present
		OMI/Aura			2005-present
	Size, shape	AVHRR/NOAA-series	Angstrom exponent	global ocean	1981-present
		POLDER-1, -2, PARASOL	fine-mode fraction, Angstrom exponent, non-spherical fraction	global land+ocean	1997-present
		MODIS/Terra, Aqua	fine-mode fraction	global land+ocean (better quality over ocean)	2000-present (Terra) 2002-present (Aqua)
			Angstrom exponent		
			Effective radius	global ocean	
			Asymmetry factor		
		MISR/Terra	Angstrom exponent Non-spherical fraction	global land+ocean	2000-present
	Absorption	TOMS/Nimbus, ADEOS1, EP	Absorbing aerosol index, single-scattering albedo, absorbing optical depth	global land+ocean	1979-2001
		OMI/Aura			2005-present
		MISR/Terra	Single-scattering albedo		2000-present
Vertical-resolved	Loading, size, and shape	GLAS/ICESat	Extinction/backscatter	global land+ocean, 16-day repeating cycle, single-nadir measurement	2003-present (~3months/year)
		CALIOP/CALIPSO	Extinction/backscatter, color ratio, depolarization ratio		2006-present

Box 2.1: MODerate resolution Imaging Spectroradiometer

MODIS performs near global daily observations of atmospheric aerosols. Seven of 36 channels (between 0.47 and 2.13 μm) are used to retrieve aerosol properties over cloud and surface-screened areas (Martins et al., 2002; Li et al., 2004). Over vegetated land, MODIS retrieves aerosol optical depth at three visible channels with high accuracy of ±0.05±0.2τ (Kaufman et al., 1997; Chu et al., 2002; Remer et al., 2005; Levy et al., 2007b). Most recently a deep-blue algorithm (Hsu et al., 2004) has been implemented to retrieve aerosols over bright deserts on an operational basis. Because of the greater simplicity of the ocean surface, MODIS has the unique capability of retrieving not only aerosol optical depth with greater accuracy, i.e., ±0.03±0.05τ (Tanré et al., 1997; Remer et al., 2002; 2005), but also quantitative aerosol size parameters (e.g., effective radius, fine-mode fraction of AOD) (Kaufman et al., 2002a; Remer et al., 2005; Kleidman et al., 2005). The fine-mode fraction has been used as a tool for separating anthropogenic aerosol from natural ones and estimating the anthropogenic aerosol direct climate forcing (Kaufman et al., 2005a,b). **Figure 2.3** shows composites of MODIS AOD and fine-mode fraction that illustrate seasonal and geographical variations of aerosol types. Clearly seen from the figure is heavy pollution over East Asia in both months, biomass burning smoke over South Africa, South America, and Southeast Asia in September, heavy dust storms over North Africa and North Atlantic in both months and over northern China in March, and a mixture of dust and pollution plume swept across North Pacific in March.

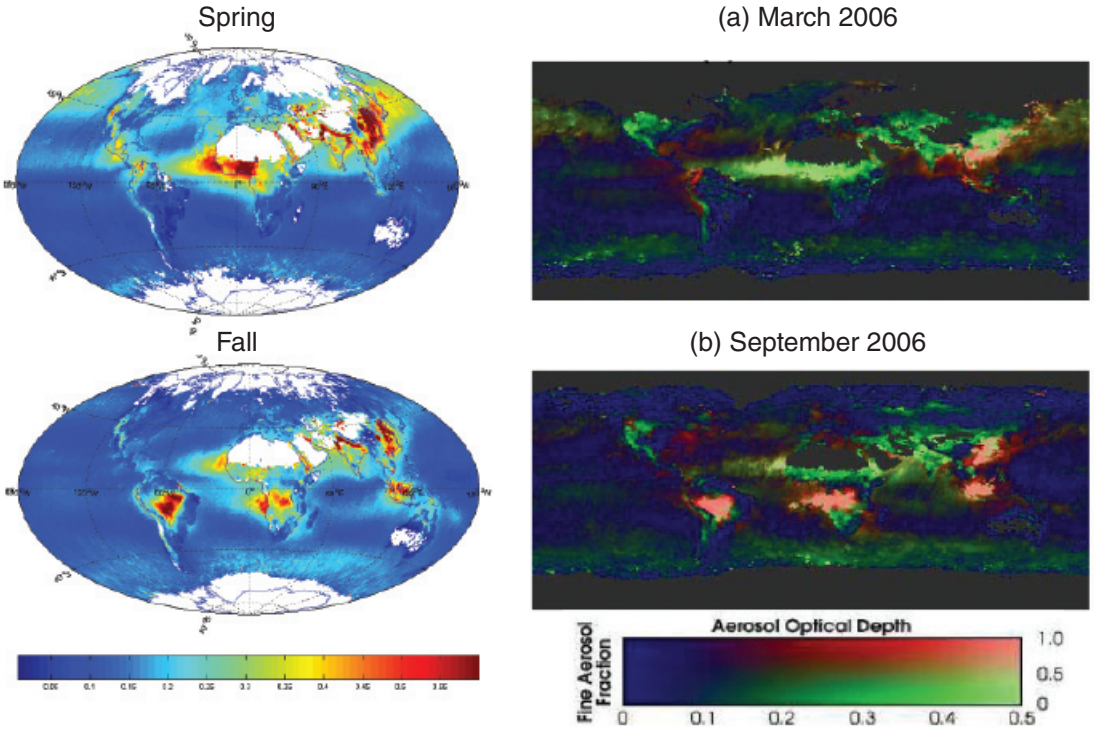

Figure 2.3: Left panel: 7-year climatology of aerosol optical depth at 550 nm. Right panel: A composite of MODIS observed aerosol optical depth (at 550 nm) and fine-mode fraction that shows spatial and seasonal variations of aerosol types. Industrial pollution and biomass burning aerosols are predominated by small particles (shown as red), while mineral dust consists of a large fraction of large particles (shown as green). Bright red and bright green indicate heavy pollution and dust plumes, respectively. The plots are generated from MODIS/Terra Collection 5 data.

Box 2.2: Multi-angle Imaging SpectroRadiometer

MISR, aboard the sun-synchronous polar orbiting satellite Terra, measures upwelling solar radiance in four visible spectral bands and at nine view angles spread out in the forward and aft directions along the flight path (Diner et al., 2002). It acquires global coverage about once per week. A wide range of along-track view angles makes it feasible to more accurately evaluate the surface contribution to the TOA radiances and hence retrieve aerosols over both ocean and land surfaces, including bright desert and sunglint regions (Diner et al., 1998; Martonchik et al., 1998a; 2002; Kahn et al., 2005a). MISR AODs are within 20% or ±0.05 of coincident AERONET measurements (Kahn et al., 2005a; Abdou et al., 2005). The MISR multi-angle data also sample scattering angles ranging from about 60˚ to 160˚ in midlatitudes, yielding information about particle size (Kahn et al., 1998; 2001; 2005a) and shape (Kalashnikova et al., 2005). These quantities are of interest in–and-of themselves for identifying aerosol airmass types, and should also help further refine aerosol retrieval algorithms. MISR also retrieves altitudes of aerosol plumes (biomass burning smoke, volcanic effluent, and mineral dust) where the plumes have discernable spatial contrast (Kahn et al., 2007). **Figure 2.4** is an example that illustrates MISR's capability of characterizing the load, optical properties, and stereo height of near-source fire plumes.

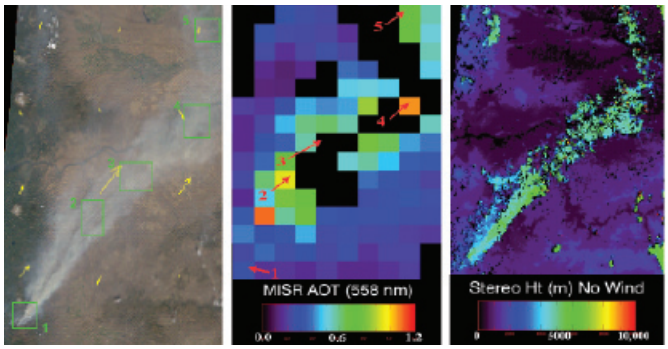

Figure 2.4: Oregon fire on September 4, 2003 as observed by MISR: (a) MISR nadir view of the fire plume, with five patch locations numbered and wind-vectors superposed in yellow; (b) MISR aerosol optical depth at 558 nm; and (c) MISR stereo height without wind correction for the same region (taken from Kahn et al., 2007).

Box 2.3: Clouds and the Earth's Radiant Energy System

CERES measures broadband solar and terrestrial radiances at three channels with a large footprint (e.g., 20 km for CERES/Terra) (Wielicki et al., 1996). It is collocated with MODIS and MISR aboard Terra and with MODIS on Aqua. The observed radiances are converted to the TOA irradiances or fluxes using the Angular Distribution Models (*ADMs*) as a function of viewing angle, sun angle, and scene type (Loeb and Kato, 2002; Zhang et al., 2005a). Such estimates of TOA solar flux in clear-sky conditions can be compared to the expected flux for an aerosol-free atmosphere, in conjunction with measurements of aerosol optical depth from other sensors (e.g., MODIS, and MISR) to derive the aerosol direct effect and climate forcing (Loeb and Manalo-Smith, 2005; Zhang and Christopher, 2003; Zhang et al., 2005b; Christopher et al., 2006). The derived instantaneous value is then scaled to obtain a daily average. A direct use of the coarse spatial resolution CERES measurements would exclude aerosol distributions in partly cloudy CERES scenes. Several approaches that incorporate coincident, high spatial and spectral resolution measurements (e.g., MODIS) have been employed to overcome this limitation (Loeb and Manalo-Smith, 2005; Zhang et al., 2005b).

Box 2.4: Active Remote Sensing of Aerosols

Following a demonstration aboard the U.S. Space Shuttle mission in 1994, the Geoscience Laser Altimeter System (GLAS) was launched in early 2003 to become the first polar orbiting satellite lidar. It provides global aerosol and cloud profiling for a one-month period out of every three-to-six months. It has been demonstrated that GLAS is capable of detecting and discriminating multiple layer clouds, atmospheric boundary layer aerosols, and elevated aerosol layers (e.g., Spinhirne et al., 2005). The Cloud-Aerosol Lidar and Infrared Pathfinder Satellite Observations (CALIPSO), launched on April 28, 2006, is carrying a lidar instrument (Cloud and Aerosol Lidar with Orthogonal Polarization - CALIOP) that has been collecting profiles of the attenuated backscatter at visible and near-infrared wavelengths along with polarized backscatter in the visible channel (Winker et al., 2003). Flying in formation with the Aqua, AURA, POLDER, and CloudSat satellites, this vertically resolved information is expected to greatly improve passive aerosol and cloud retrievals as well as allow the development of new retrieval products (see Kaufman et al., 2003; Léon et al., 2003).

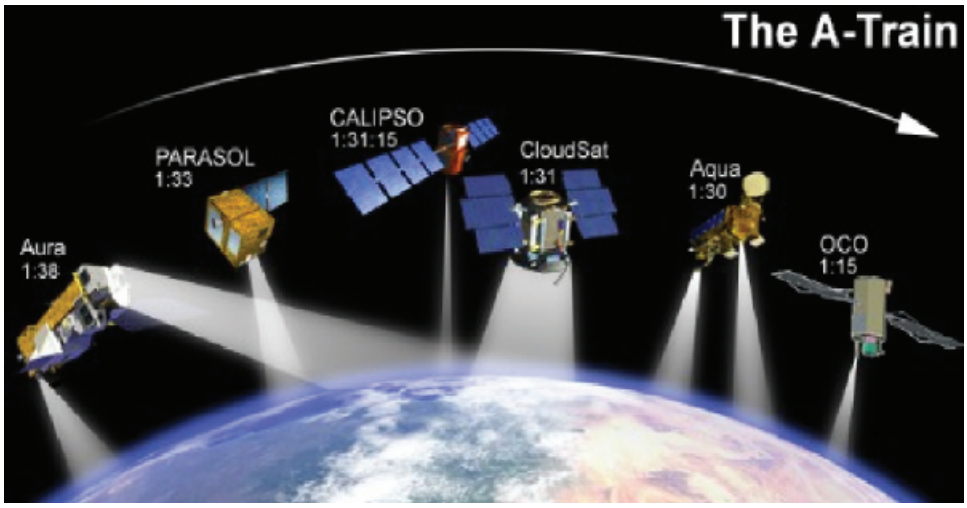

Figure 2.2: A constellation of six spacecrafts with afternoon overpass, so-called A-Train, will provide an unprecedented opportunity of studying aerosols and clouds from the space in multiple dimensions with sensors with complimentary capabilities. The formation of A-Train is expected to complete when OCO is launched in 2008.

The high accuracy of aerosol products (mainly aerosol optical depth) from these new-generation sensors, together with improvements in characterizing the earth's surface and clouds, can help reduce the uncertainties associated with the aerosol direct radiative effect (Yu et al., 2006; and references therein). The retrieved aerosol size parameters can help distinguish anthropogenic aerosols from natural aerosols and hence help assess the anthropogenic aerosol radiative forcing (Kaufman et al., 2005a, b; Bellouin et al., 2005; Christopher et al., 2006; Yu et al., 2006).

Finally, algorithms are being developed to retrieve aerosol absorption or single-scattering albedo from satellite observations (e.g., Kaufman et al., 2002b; Torres et al., 2005). The NASA Glory mission, scheduled to launch in 2008 and to be added to the A-Train, will deploy a multi-angle, multi-spectral polarimeter to determine the global distribution of aerosol and clouds. It will also be able to infer microphysical properties, and chemical composition by source type (e.g., marine, dust, pollution, etc.) of aerosols with accuracy and coverage sufficient for improving quantification of the aerosol direct and indirect effects on climate (Mishchenko et al., 2007b).

2.2.4. *Synergy of Measurements and Model Simulations*

As discussed earlier, aerosols and their climate forcing have been observationally studied through the establishment and enhancement of ground-based networks, the development and implementation of new and enhanced satellite sensors, and the execution of intensive field experiments. However, none of these approaches alone is adequate to characterize large spatial and temporal variations of aerosol physical and chemical properties and to address complex aerosol-climate interactions. Individual approaches have their own strengths and limitations, and are usually complementary. For example, while ground-based networks and intensive field experiments provide the most accurate information about aerosol properties that is required for evaluating and constraining satellite retrievals and model simulations, they are lacking in spatial and/or temporal coverage. Satellite remote sensing can augment the ground networks and field experiments by expanding the temporal and spatial coverage, but can only offer limited retrievable parameters (as determined by sensor's wavelength channels, viewing angles, and polarization capability) and usually only under cloud free conditions. Therefore, the best strategy for characterizing aerosols is to integrate measurements from different satellite sensors with complementary capabilities from sub-orbital measurements.

Models are versatile, although imperfect tools for studying aerosols in both clear and cloudy conditions and providing information on chemical composition that can not be directly observed from satellites. Model simulation is also an indispensable tool for estimating past aerosol forcing and projecting future climate due to changes in atmospheric aerosols. On the other hand, model simulations have large uncertainties because of the difficulties in realistically representing the aerosol life cycle. Along with improving representation of various processes within models, observations are essential for constraining model simulations of aerosol climate impacts through data synthesis.

In the following, we discuss several synergistic approaches to studying aerosols and their climate forcing, including closure studies involving multiple independent data sets, constraint of model aerosol optical properties with in-situ measurements, and integration of satellite observations into models.

Closure Studies: During intensive field experiments, multiple platforms and instruments are deployed to sample the same air mass through a well-coordinated experimental design. Often, several different independent methods are used to measure or derive a single aerosol property or radiative effect. This combination of methods can be used to identify inconsistencies in the measurements and to quantify uncertainties in aerosol characterization and estimates of aerosol radiative effects. This approach, often referred to as a closure study, has been widely employed on both individual measurement platforms (local closure) and in studies involving vertical measurements through the atmospheric column by one or more platforms (column closure) (Quinn et al., 1996; Russell et al., 1997).

As summarized in Bates et al. (2006), aerosol closure studies reveal that the best agreement between measurements occurs for submicrometer, spherical aerosol particles. For submicrometer sulfate/carbonaceous aerosol, measurements of aerosol optical properties and optical depths agree within 10 to 15% and often better. Larger particle sizes present inlet collection efficiency difficulties and non-spherical particles (e.g., dust) lead to differences in instrumental response. Comparisons of optical depth for an aerosol dominated by dust reveal disagreements between methods of up to 35%. Closure studies on DRE reveal uncertainties of about 25% for sulfate/carbonaceous aerosol and 60% for dust. Future

closure studies are needed to integrate surface- and satellite-based radiometric measurements of AOD with in-situ optical, microphysical, and aircraft radiometric measurements. There is also a need to maintain consistency in comparing results and expressing uncertainties (Bates et al., 2006).

Constraining models with in-situ measurements: In-situ measurements of aerosol chemical, microphysical, and optical properties, with a known accuracy based, in part, on closure studies, can be used to constrain regional CTM simulations of aerosol DRE and DCF, as described by Bates et al. (2006). A key step in the approach is assigning empirically derived optical properties to the individual chemical components generated by the CTM for use in a Radiative Transfer Model (RTM). Specifically, regional data from focused, short-duration field programs can be segregated according to aerosol type (sea salt, dust, or sulfate/carbonaceous) based on measured chemical composition and particle size. Corresponding measured optical properties can be carried along in the sorting process so that they, too, are segregated by aerosol type. The so-derived intensive aerosol properties for individual aerosol types, including mass scattering efficiency, single-scattering albedo, and asymmetry factor, and their dependences on relative humidity, are used in place of *a priori* values in CTMs. Bates et al. (2006) show that such constraint leads to about a 30% increase in DRE and DCF estimates in a regional and a global CTM, compared to model calculations based on *a priori* optical properties. Data from short-term, focused experiments are limited in their ability to constrain model-simulated extensive properties of aerosols, such as concentration and AOD, as these properties are much more heterogeneous in space and time than the intensive properties. Long-term in-situ measurements as well as satellite observations are more suited for constraining extensive aerosol properties.

Integration of satellite measurements into model simulations: Global measurements of aerosols (mainly AOD) from satellites can also be used to improve the performance of aerosol model simulations and hence the assessment of the aerosol direct radiative effect through data assimilation or objective analysis process (e.g., Collins et al., 2001; Yu et al., 2003; 2004, 2006; Liu et al., 2005). Both satellite retrievals and model simulations have uncertainties. The goal of data integration is to minimize the discrepancies between them, and to form an optimal estimate of aerosol distributions by combining them with weights inversely proportional to the square of the errors of individual descriptions. Such integration can fill gaps in satellite retrievals and generate global distributions of aerosols that are consistent with ground-based measurements (Collins et al., 2001; Yu et al., 2003, 2006; Liu et al., 2005). Recent efforts have focused on retrieving global sources of aerosol from satellite observations using inverse modeling which may be potentially valuable for reducing large uncertainties of aerosol simulations (Dubovik et al., 2007).

2.3. Assessments of Aerosol Characterization and Climate Forcing

In this section we focus on the assessment of measurement-based aerosol characterization and its use in improving estimates of the direct radiative effect and climate forcing on regional and global scales. In-situ measurements provide highly accurate aerosol chemical, microphysical, and optical properties on a regional basis and for the particular time period of a given experiment. Remote sensing from satellites and ground-based networks provide spatial and temporal coverage that intensive field campaigns lack. Both in-situ measurements and remote sensing have been used to determine key parameters for estimating aerosol direct climate forcing including aerosol single scattering albedo, asymmetry factor, optical depth, and direct radiative effect. Remote sensing has also been providing simultaneous mea-

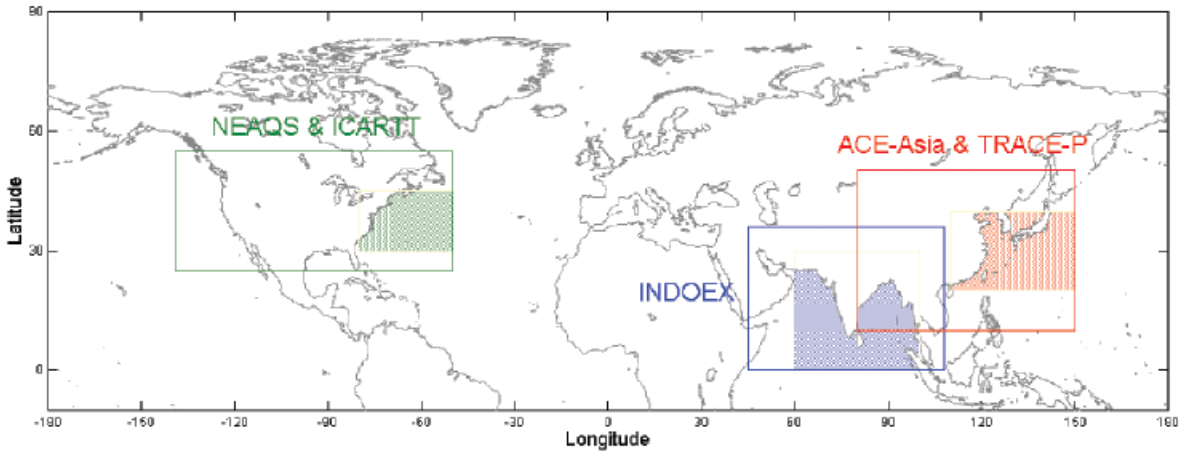

Figure 2.5. Locations of field campaigns that served as the source of data used to constrain model estimates of DRE and DCF in the Bates et al. (2006) study. Solid boxes show the regional CTM domains. Shaded areas show the regions use for the DRE and DCF calculations.

surements of aerosol and radiative fluxes that can be combined to derive aerosol direct radiative effect and climate forcing at the TOA with relaxed requirement for characterizing aerosol intensive properties. We also discuss progress in using both satellite and surface-based remote sensing measurements to study aerosol-cloud interactions and indirect effects.

2.3.1. *The Use of Regional Aerosol Chemical and Optical Properties to Improve Model Estimates of DRE and DCF*

The wide variety of aerosol data sets from intensive field campaigns provide a rigorous "test bed" for model simulations of aerosol distributions and estimates of DRE and DCF, as demonstrated in Bates et al. (2006). The approach taken by Bates et al. to constrain estimates of DRE and DCF is as follows. CTMs were used to calculate dry mass concentrations of the dominant aerosol species (sulfate, organic carbon, black carbon, sea salt, and dust). In-situ measurements were used to calculate the corresponding optical properties for each aerosol type for use in a radiative transfer model (RTM). Aerosol DRE and DCF estimated by using the empirically derived and a priori optical properties were then compared. In addition, in-situ and ground-based remote measurements were used to check or validate both the CTM and the RTM output.

Here we discuss the details of the aerosol chemical and optical properties in the three regions considered by Bates et al. (see **Figure 2.5**) and the use of these empirically-determined properties in improving model estimates of aerosol burdens, DRE, and DCF. These regions include:

- the Northern Indian Ocean (NIO) where INDOEX took place in 1999.
- the Northwestern Pacific Ocean (NPO) where ACE-Asia took place in 2001.
- the Northwestern Atlantic Ocean (NWA) where the New England Air Quality Study (NEAQS-2002) occurred in 2002 and ICARTT occurred in 2004.

The NIO, NPO, and NWA each have distinct aerosol properties due to differences in upwind sources. Variability in aerosol mass concentration and chemical composition for the three regions is shown

in **Figure 2.6** for the submicrometer (aerodynamic diameter between 0.1 and 1 μm) and supermicrometer (aerodynamic diameter between 1 and 10 μm) aerosol. The data in Figure 6 are based on measurements onboard the NOAA RV *Ronald H. Brown* using standardized sampling protocols which minimizes sampling biases and, hence, allows for a direct comparison of the data from all three experiments (Quinn and Bates, 2005).

Although the mean submicrometer aerosol mass concentrations were similar between the three regions (15 to 20 μg m^{-3}), the aerosol composition differed. INDOEX took place during the dry winter monsoon season, which is characterized by large-scale subsidence and northeasterly flow from the Indian subcontinent to the northern Indian Ocean. Submicrometer aerosol was dominated by sulfate and dust/fly ash with a significant contribution from BC. Emissions of BC from India result primarily from residential combustion (biofuel) with contributions from industry and transportation.

ACE-Asia took place during the spring when dust outbreaks over the Gobi desert are most frequent and intense. The submicrometer aerosol measured during ACE-Asia was primarily sulfate, POM, and dust while the supermicrometer aerosol was dominated by dust. The large supermicrometer mass concentrations measured during ACE-Asia indicate the large aerosol loadings that result from the springtime dust outbreaks.

Sub-micrometer aerosol mass concentrations measured during ICARTT were uniquely dominated by POM and sulfate. Based on modeling studies and statistical comparisons to gas phase volatile organic tracer compounds, the POM appears to be mainly of anthropogenic origin (de Gouw et al., 2005; Quinn et al., 2006).

Several factors contribute to the uncertainty of CTM calculations of size distributed aerosol composition including emissions, aerosol removal by wet deposition, chemical processes involved in the

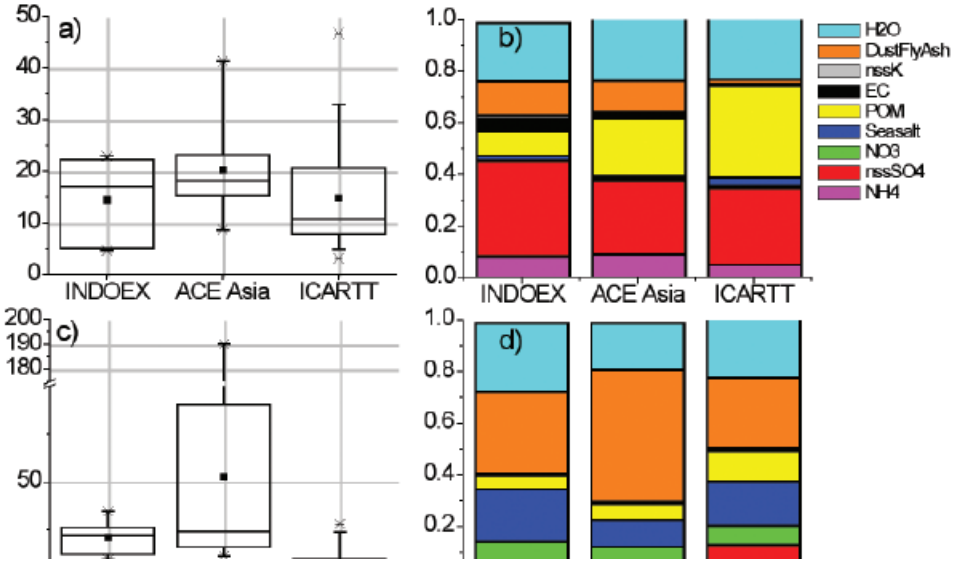

Figure 2.6: Submicrometer aerosol a) mass concentrations and b) mass fractions of the dominant chemical components measured during INDOEX, ACE-Asia, and ICARTT onboard Ronald H. Brown. Similarly, supermicrometer aerosol c) mass concentrations and d) mass fractions of the dominant chemical components measured during INDOEX, ACE-Asia, and ICARTT onboard Ronald H. Brown. Values are shown at the measurement RH of 55±5%.

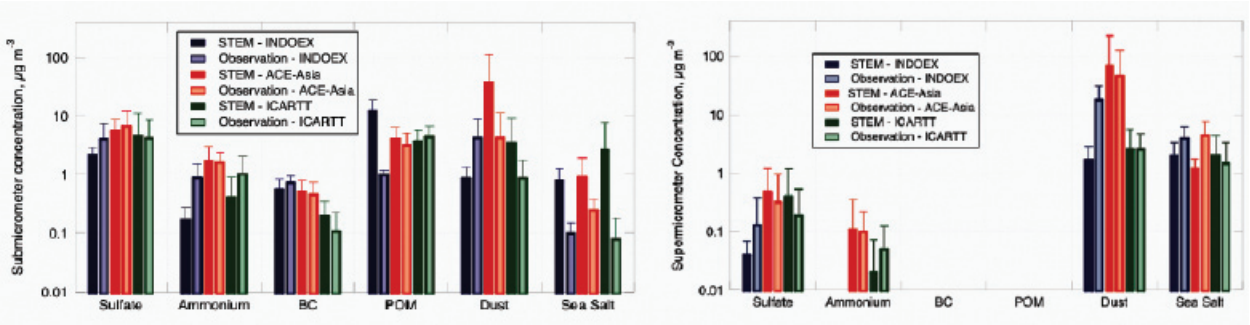

Figure 2.7: Comparison of the mean concentration (μg m^{-3}) and standard deviation of the modeled (STEM) aerosol chemical components with those observed on the RV Ronald H. Brown during INDOEX, ACE-Asia, and ICARTT. After Bates et al. (2006).

formation of secondary aerosols, vertical transport, and meteorological fields including the timing and amount of precipitation, formation of clouds, and relative humidity. In-situ measurements made during the intensive field campaigns described above provide a point of comparison for the CTM generated aerosol distributions at the surface and at discrete points above the surface. Such comparisons are useful for identifying areas where the models need improvement.

The submicrometer, supermicrometer, and sub-10 micrometer aerosol chemical components measured during INDOEX, ACE-Asia, and ICARTT are compared with those calculated with the Sulfate Transport and dEposition Model (*STEM*) (e.g., Carmichael et al., 2002, 2003; Tang et al., 2003, 2004; Bates et al., 2004; Streets et al., 2006a), as shown in **Figure 2.7**. To directly compare the measured (*RV Ronald H. Brown*) and modeled values, the model was sampled at the times and locations of the shipboard measurements every 30 min along the cruise track. The best agreement is found for submicrometer sulfate and BC. Large discrepancies between the modeled and measured values occur for submicrometer POM (INDOEX), dust (ACE-Asia), and sea salt (all regions). In the super-micrometer size range, large disagreements occur for dust (INDOEX) and sea salt (INDOEX and ACE-Asia). The total mass of the supermicrometer aerosol is underestimated by the model by about a factor of 3.

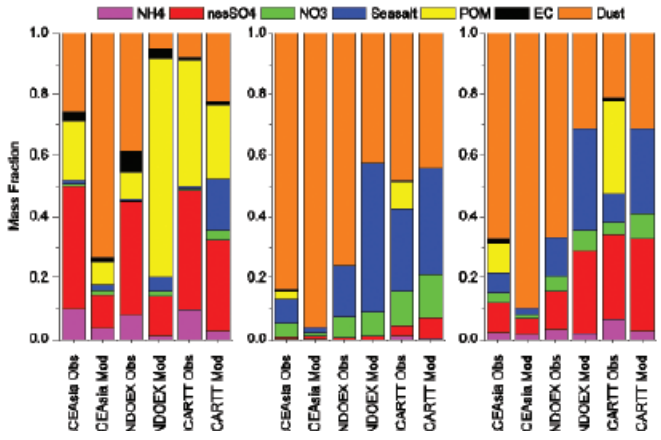

Figure 2.8. Mass fractions of the aerosol chemical components for INDOEX, ACE-Asia, and ICARTT based on shipboard measurements and STEM model calculations. Left panel is submicrometer aerosol, middle panel is supermicrometer aerosol, and right panel is sub-10 micrometer aerosol. After Bates et al. (2006).

A comparison of the modeled and measured mass fractions of the chemical components for the three size ranges is shown in **Figure 2.8**. The model is able to duplicate the measurements to the degree that the sub-micrometer aerosol is composed of a mixture of sulfate, POM, and BC and the supermicrometer aerosol is composed primarily of dust and sea salt. The relative amount of each component is not well-captured by the model for either size range, however. Discrepancies in the measured and modeled dust and sea salt concentrations and mass fractions reflect the large uncertainties in the emission models used for the components. Uncertainties in the column amounts of sea salt and dust are significant as both compo-

nents contribute substantially to AOD and DRE. In addition, both of these components can interact with gas and particle phase species thereby impacting concentrations and size distributions of anthropogenic aerosol components.

Further comparisons made by Bates et al. (2006) between STEM and aircraft-derived component concentrations revealed that 1) model results are better at altitudes less than 2 km due to the uncertainties in modeling vertical transport and removal processes; 2) dust and sea salt are underestimated, likely due to errors in model-calculated emissions and parameterizations of removal processes; and 3) the agreement is best for sulfate due to greater accuracy in emissions, chemical conversion, and removal for this component.

Empirically determined optical properties of interest in the calculation of DRE and DCF are compared for the three regions in **Figure 2.9**. The dependence of these parameters on particle size (submicrometer vs. super-micrometer) and wavelength (450, 550, and 700 nm) is indicated. Single scattering albedo shows a strong dependence on both wavelength and particle size. Values are the lowest for sub-micrometer aerosol measured during INDOEX which corresponds with the relatively large sub-micrometer BC mass fractions observed in NIO region (as shown in Figure 7). Although there is a strong wavelength-dependence of aerosol scattering efficiency, values of mass scattering efficiency are similar among the three geographical regions, indicating that the variability in aerosol size distribution (modal diameter and width) or particle shape is not large enough to lead to significant regional differences (Quinn and Bates, 2005). The hemispheric backscattered fraction, b, derived from measurements made with an integrating nephelometer, is a complex function of particle size and shape.

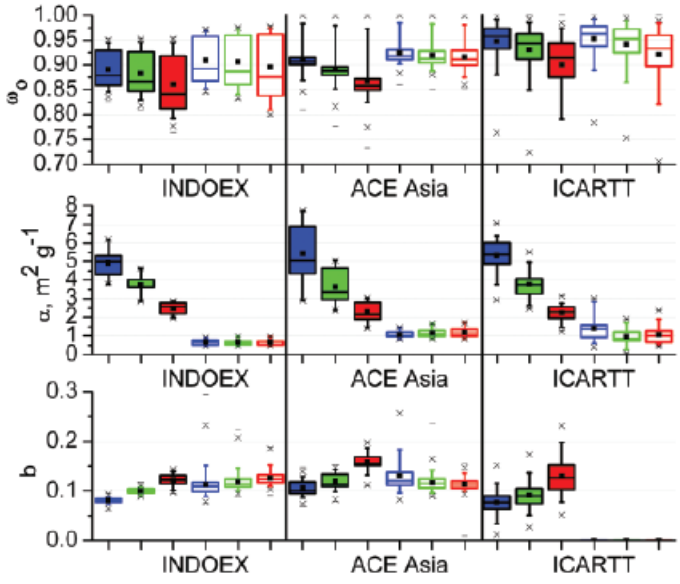

Figure 2.9: Mean and variability in single scattering albedo (ω_o), mass scattering efficiency (α), and backscattered fraction (b) for INDOEX, ACE-Asia, and ICARTT. Submicrometer values are solid bars, supermicrometer values are open bars. Wavelength is indicated by color (blue = 450 nm, green = 550 nm, red = 700 nm). The horizontal lines in the box denote the 25th, 50th, and 75th percentiles. The whisker denotes the 5th and 95th percentiles. The x denotes the 1st and 99th percentile. The square denotes the mean. Values are shown at the measurement RH of 55 ± 5%.

While the data discussed here (chemical composition shown in **Figure 2.6** and optical properties shown in **Figure 2.9**) are representative of conditions in the marine boundary layer during intensive field campaigns, they can be extended to cover a broader spatial and temporal scale through comparisons with surface-based observations and aircraft data during the campaigns, as well as long-term surface network measurements (Bates et al., 2006).

A key step in the Bates et al. approach is assigning empirically derived optical properties to the individual chemical components generated by the CTM for use in the RTM. Carrying the individual components through the RTM calculations (rather than the total aerosol) is required to attribute DRE and DCF to specific aerosol components. However, aerosol optical properties measured during field campaigns are, in general, characteristic of the total aerosol, not the individual species. In order to use the measurements to derive optical properties of individual components, the following assumptions were made: 1) aerosol mass over the ocean regions is present in an accumulation and a coarse mode, 2) sea salt and/or dust are present as external mixtures in the coarse mode (or supermicrometer size range), and 3) sulfate, OC, BC, and ammonium are internally mixed and exist entirely in the accumulation mode (submicrometer size range). Data for the NIO, NWP and NWA were segregated according to aerosol type (sea salt, dust, or sulfate/carbonaceous) based on measured chemical composition and particle size thereby isolating the sulfate/carbonaceous accumulation mode aerosol from the dust and sea salt coarse mode. Measured optical properties were carried along in the sorting process so that they, too, were segregated by aerosol type. As a result of this analysis, optical properties were estimated based on measurements as a function of aerosol size, type (composition), relative humidity, and wavelength.

One outcome of the Bates et al. analysis was a formal parameterization of the enhancement in light scattering due to the uptake of water vapor by aerosol particles [$f_{\sigma sp}(RH)$] for sulfate/carbonaceous aerosol mixtures. Prior to this analysis, both model and measurement studies revealed that POM internally mixed with water soluble salts can reduce the hygroscopic response of the aerosol, which decreases its water content and ability to scatter light at elevated relative humidities (e.g., Saxena et al., 1995; Carrico et al., 2005). Measurements made during INDOEX, ACE-Asia, and ICARTT revealed a substantial decrease in $f_{\sigma sp}(RH)$ with an increasing mass fraction of POM in the accumulation mode. Based on these data, a relationship between $f_{\sigma sp}(RH)$ and the POM mass fraction was developed for accumulation mode sulfate-POM aerosol (Quinn et al., 2005). The relationship is given by

$$f_{\sigma sp}(RH, RH_{ref}) = \sigma_{sp}(\mathrm{RH})/\sigma_{sp}(\mathrm{RH_{ref}}) = [(100 - \mathrm{RH_{ref}})/(100 - \mathrm{RH})]^{\gamma s} \qquad (1)$$

where

$$\gamma_s = 0.9 - 0.6*F_O \qquad (2)$$

and

$$F_o = C_O/(C_O + C_S) \qquad (3).$$

C_O and C_S are the measured mass concentrations of submicrometer POM and sulfate, respectively. The radiative transfer calculations of Bates et al. used the CTM output of C_O and C_S in Equation (3) to determine γ_s.

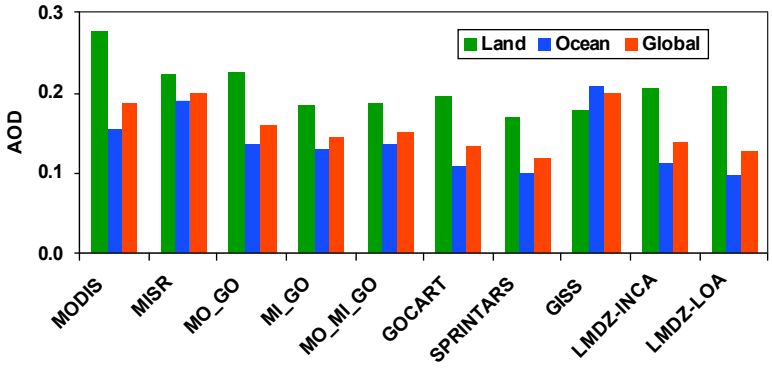

Figure 2.10: Comparison of annual mean aerosol optical depth (AOD) at 550 nm between satellite retrievals, model simulations, and satellite-model integrations averaged over land, ocean, and globe (all limited to 60°S-60°N region) (figure generated from Table 6 in Yu et al., 2006).

To compare the results using the *a priori* and empirically-derived optical properties, Bates et al. calculated DRE and DCF once using the optical properties built into the radiation code (*a priori*) and once using the observed properties (constrained). In addition, two RTMs (GFDL AM2 (GAMDT, 2004) and the University of Michigan (Liu et al., 2007)) were run with input from two different CTMs (STEM and MOZART). Results of the comparison of *a priori* versus constrained RTM runs include the following. The constrained optical properties derived from measurements increased the calculated AOD (34 ± 8%), TOA DRE (32 ± 12%), and TOA DCF (37 ± 7%) relative to runs using the *a priori* values. These increases are due to the larger values of the constrained mass extinction efficiencies relative to the *a priori* values. In addition, differences in AOD due to using the aerosol loadings from MOZART versus those from STEM are much greater than differences resulting from the *a priori* vs. constrained RTM runs. This result reflects the fact that DRE and DCF are linearly proportional to the amount of aerosol present.

The use of empirically-derived aerosol properties to assess model output (both CTM and RTM) and to serve as input to RTM calculations revealed that 1) uncertainties in calculated AOD and DRE are large and due primarily to the large uncertainties in the emissions and burdens of dust and sea salt, 2) the choice of aerosol optical properties (a priori or constrained) is a much smaller source of uncertainty in estimates of AOD, DRE, and DCF than is the choice of chemical transport model that determines the aerosol field for use in the radiative transfer calculations, and 3) the use of constrained optical properties led to values of AOD that were about 30% larger than those based on *a priori* optical properties. Similarly, the use of constrained optical properties led to about a 30% increase in TOA DRE and DCF indicating that AOD, DRE, and DCF, for these experimental regions, may be greater than previously estimated.

2.3.2. *Intercomparisons of Satellite Measurements and Model Simulation of Aerosol Optical Depth*

Given the fact that DRE and DCF are proportional to the amount of aerosol present, it is of first order importance to improve the spatial characterization of aerosol optical depth (AOD) on a global scale. This requires an evaluation of the various remote sensing data sets of AOD and comparison with model-estimates of AOD. The latter comparison is particularly important if we are to use models to predict future climate states. Both remote sensing and model simulation have uncertainties and satellite-model integration is needed to obtain an optimum description of aerosol distribution.

Figure 2.10 shows an intercomparison of annual average aerosol optical depth at 550 nm from two recent aerosol-oriented satellite sensors (MODIS and MISR), five model simulations (GOCART, GISS,

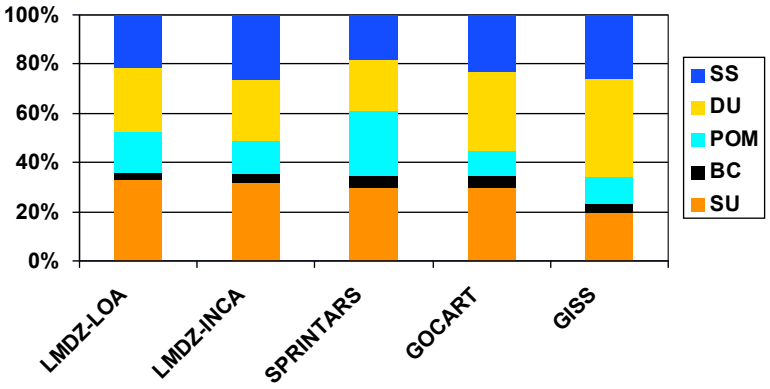

Figure 2.11: Percentage contributions of individual aerosol components (SU – sulfate, BC – black carbon, POM – particulate organic matter, DU – dust, SS – sea-salt) to the total aerosol optical depth (at 550 nm) on a global scale simulated by the five models (data taken from Kinne et al., 2006).

SPRINTARS, LMDZ-LOA, LMDZ-INCA) and three satellite-model integrations (MO_GO, MI_GO, MO_MI_GO). These model-satellite integrations are conducted by using an optimum interpolation approach (Yu et al., 2003) to constrain GOCART simulated AOD with that from MODIS, MISR, or MODIS over ocean and MISR over land, denoted as MO_GO, MI_GO, and MO_MI_GO, respectively. MODIS values of AOD are from Terra Collection 4 retrievals and MISR AOD is based on early post launch retrievals. MODIS and MISR retrievals give a comparable average AOD on the global scale, with MISR greater than MODIS by 0.01~0.02 depending on the season. However, differences between MODIS and MISR are much larger when land and ocean are examined separately: AOD from MODIS is 0.02-0.07 higher over land but 0.03-0.04 lower over ocean than the AOD from MISR. These differences are being reduced by the new MODIS aerosol retrieval algorithms in Collection 5 (Levy et al., 2007b) and the improved radiance calibration in MISR retrievals (Kahn et al., 2005b).

The annual and global average AOD from the five models is 0.19±0.02 (mean ± standard deviation) over land and 0.13±0.05 over ocean, respectively. Clearly, the model-based mean AOD is smaller than both MODIS- and MISR-derived values (except the GISS model). A similar conclusion has been drawn from more extensive comparisons involving more models and satellites (Kinne et al., 2006). On regional scales, satellite-model differences are much larger. These differences could be attributed, in part, to cloud contamination and 3D cloud effects in satellite retrievals (Kaufman et al., 2005b; Wen et al., 2006) or to models missing important aerosol sources/sinks or physical processes (Koren et al., 2007a). The satellite-model integrated products are generally in-between the satellite retrievals and the model simulations, and agree better with AERONET measurements (e.g., Yu et al., 2003).

As in the case of in-situ/model comparisons, there appears to be a relationship between uncertainties in the representation of dust in models and the uncertainty in AOD, and its global distribution. For example, the GISS model generates more dust than the other models (Fig. 2.11), resulting in a closer agreement with MODIS and MISR in the global mean (Fig. 2.10). However, the distribution of AOD between land and ocean is quite different from MODIS- and MISR-derived values.

Figure 2.11 shows larger model differences in the simulated percentage contributions of individual components to the total aerosol optical depth on a global scale, and hence in the simulated aerosol single-scattering properties (e.g., single-scattering albedo, and phase function), as documented in Kinne et al. (2006). This, combined with the differences in aerosol loading (i.e., optical depth) determines the model diversity in simulated aerosol direct radiative effect and forcing, as discussed later.

However, current satellite remote sensing capability is not sufficient to constrain model simulations of aerosol components.

2.3.3. *Remote Sensing Based Estimates of Aerosol Direct Radiative Effect*

AERONET and other surface networks usually provide a set of aerosol optical properties that can be used to calculate the aerosol direct radiative effect (Procopio et al., 2004; Zhou et al., 2005). The calculated aerosol radiative effect can be used to evaluate both satellite remote sensing measurements and model simulations (e.g., Yu et al., 2006). **Figure 2.12** shows the diurnally averaged, normalized aerosol direct effect based on the AERONET data that represent different aerosol types, geographical locations, and surface properties (Zhou et al., 2005). The normalized aerosol direct effect is referred to as *radiative efficiency* (E_τ), defined as a ratio of DRE to τ at 550 nm (Anderson et al., 2005a). The quantity of E_τ is mainly governed by aerosol size distribution and chemical composition (determining the aerosol single-scattering albedo and phase function), surface reflectivity, and solar irradiance, and also to some degree depends on the optical depth because of multiple scattering. The figure demonstrates how the aerosol direct solar effect is determined by a combination of aerosol and surface properties. For example, the radiative effect by South African biomass burning smoke differs significantly from that by South American smoke because of the much stronger light absorption due to smoke generated in South Africa (Dubovik et al., 2002; Eck et al., 2003). Mineral dust from North Africa and the Arabian Peninsula exert a radiative perturbation with a factor of ~2 difference in magnitude, due mainly to considerable spatial variability of surface reflectance in the region (Tsvetsinskaya et al., 2002).

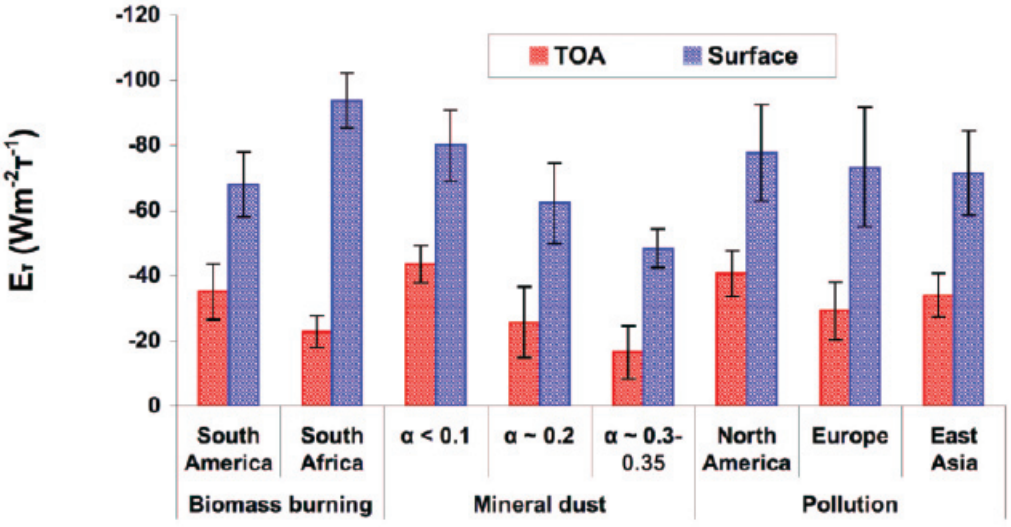

Figure 2.12: The clear-sky radiative efficiency E_τ, defined as the aerosol direct radiative effect (W m^{-2}) per unit aerosol optical depth (τ) at 550 nm, at the TOA and the surface for typical aerosol types and over different geographical regions, which is calculated from AERONET aerosol climatology. The vertical bars represent one standard deviation of Eτ for individual aerosol regimes. α is surface broadband albedo. The figure demonstrates how the aerosol direct solar effect is determined by a combination of aerosol and surface properties. The radiative effect by South African biomass burning smoke differs significantly from that by South America smoke because of stronger absorption of smoke in South Africa. Mineral dust from North Africa and the Arabian Peninsula exerts much different magnitude of radiative perturbation due mainly to considerable spatial variability of surface reflectance in the region (adapted from Zhou et al., 2005)

Table 2.4: Summary of approaches to estimating the aerosol direct radiative effect in three categories: (A) satellite retrievals; (B) satellite-model integrations; and (C) model simulations. (adapted from Yu et al., 2006)

Category	Product	Brief Descriptions	Identified Sources of Uncertainty	Major References
A. Satellite retrievals	MODIS	Using MODIS retrievals of a linked set of AOT, ω_0, and phase function consistently in conjunction with a radiative transfer model (RTM) to calculate TOA fluxes that best match the observed radiances.	Radiance calibration, cloud-aerosol discrimination, instantaneous-to-diurnal scaling, RTM parameterizations	Remer and Kaufman, 2006
	MODIS_A	Splitting MODIS AOD over ocean into mineral dust, sea-salt, and biomass-burning and pollution; using AERONET measurements to derive the size distribution and single-scattering albedo for individual components.	Satellite AOD and FMF retrievals, overestimate due to summing up the compositional direct effects, use of a single AERONET site to characterize a large region	Bellouin et al., 2005
	CERES_A	Using CERES fluxes in combination with standard MODIS aerosol	Calibration of CERES radiances, large CERES footprint, satellite AOD retrieval, radiance-to-flux conversion (ADM), instantaneous-to-diurnal scaling, narrow-to-broadband conversion	Loeb and Manalo-Smith, 2005 ; Loeb and Kato, 2002
	CERES_B	Using CERES fluxes in combination with NOAA NESDIS aerosol from MODIS radiances		
	CERES_C	Using CERES fluxes in combination with MODIS aerosol with new angular models for aerosols		Zhang et al, 2005a,b ; Zhang and Christopher, 2003; Christopher et al., 2006
	POLDER	Using POLDER AOD in combination with prescribed aerosol models (similar to MODIS)	Similar to MODIS	Boucher and Tanré, 2000 ; Bellouin et al., 2003
B. Satellite-model integrations	MODIS_G	Using GOCART simulations to fill AOD gaps in satellite retrievals	Propagation of uncertainties associated with both satellite retrievals and model simulations (but the model-satellite integration approach does result in improved AOD quality for MO_GO, and MO_MI_GO)	* Aerosol single-scattering albedo and asymmetry factor are taken from GOCART simulations; * Yu et al, 2003, 2004, 2006
	MISR_G			
	MO_GO	Integration of MODIS and GOCART AOT		
	MO_MI_GO	Integration of GOCART AOD with retrievals from MODIS (Ocean) and MISR (Land)		
	SeaWiFS	Using SeaWiFS AOD and assumed aerosol models	Similar to MODIS_G and MISR_G, too weak aerosol absorption	Chou et al, 2002
C. Model simulations	GOCART	Offline RT calculations using monthly average aerosols with a time step of 30 min (without the presence of clouds)	Emissions, parameterizations of a variety of sub-grid aerosol processes (e.g., wet and dry deposition, cloud convection, aqueous-phase oxidation), assumptions on aerosol size, absorption, mixture, and humidification of particles, meteorology fields, not fully evaluated surface albedo schemes, RT parameterizations	Chin et al., 2002; Yu et al., 2004
	SPRINTARS	Online RT calculations every 3 hrs (cloud fraction=0)		Takemura et al, 2002, 2005
	GISS	Online model simulations and weighted by clear-sky fraction		Koch and Hansen, 2005; Koch et al., 2006
	LMDZ-INCA	Online RT calculations every 2 hrs (cloud fraction = 0)		Balkanski et al., 2007; Schulz et al., 2006; Kinne et al., 2006
	LMDZ-LOA	Online RT calculations every 2 hrs (cloud fraction=0)		Reddy et al., 2005a, b

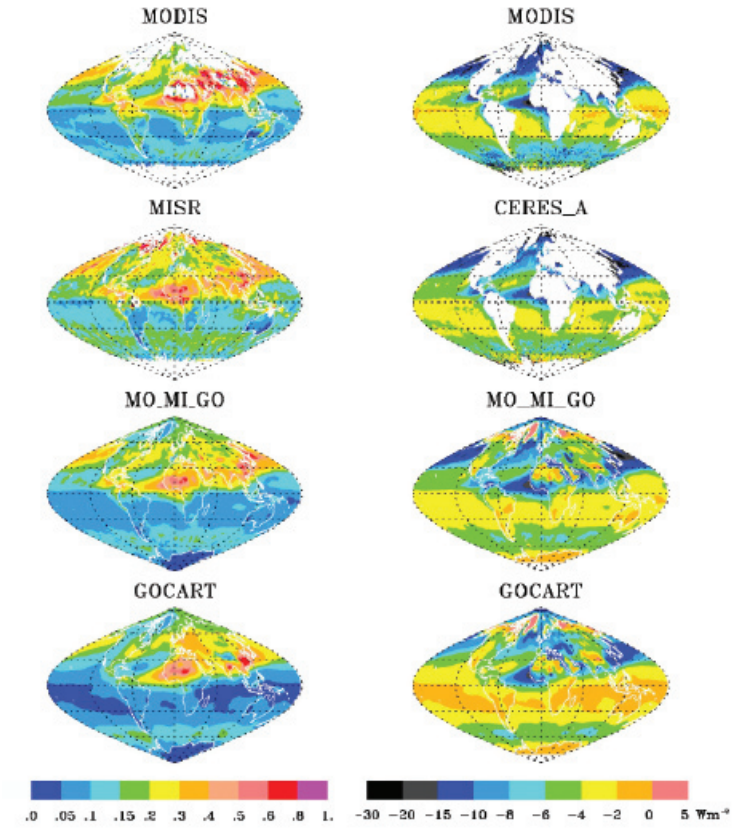

Figure 2.13: Geographical patterns of seasonally (MAM) averaged aerosol optical depth at 550 nm (left panel) and the diurnally averaged clear-sky aerosol direct solar effect (Wm-2) at the TOA (right panel) derived from satellite (Terra) retrievals (MODIS, Remer et al., 2005; Remer and Kaufman, 2006; MISR, Kahn et al., 2005a; and CERES_A, Loeb and Manalo-Smith, 2005), GOCART simulations (Chin et al., 2002; Yu et al., 2004), and GOCART-MODIS-MISR integrations (MO_MI_GO, Yu et al., 2006) (taken from Yu et al., 2006).

Table 2.4 summarizes approaches to estimating the aerosol direct solar effect, including a brief description of methods, identifies major sources of uncertainty, and provides references. These estimates fall into three broad categories, namely (A) satellite-based, (B) satellite-model integrated, and (C) model-based. Since satellite aerosol measurements are generally limited to cloud-free conditions, we focus here on assessments of clear-sky aerosol direct radiative effect and forcing and defer a discussion on complex influences of clouds on the aerosol direct effect and forcing to section 2.4.

Figure 2.13 shows global distributions of aerosol optical depth at 550 nm (left panel) and diurnally averaged clear-sky direct radiative effect at the TOA (right panel) for March-April-May (MAM) based on the different approaches. The direct effect at the surface follows the same pattern as that at the TOA but is significantly larger in magnitude because of aerosol absorption. It appears that different approaches agree on large-scale patterns of aerosol optical depth and the direct effect on solar radiation. In this season, the aerosol impacts in the Northern Hemisphere are much larger than those in the Southern Hemisphere. Dust outbreaks and biomass burning elevate the optical depth to more than 0.3 in large parts of North Africa and the tropical Atlantic. In the tropical Atlantic, TOA cooling as large as -10 Wm^{-2} extends westward to Central America. In highly polluted eastern China, the optical depth is as high as 0.6-0.8, resulting from the combined effects of pollution and biomass burning in the south, and dust outbreaks in the north. The impacts from Asia also extend to the North Pacific, with a TOA cooling of more than -10 Wm^{-2}. Other areas with large aerosol impacts include Western Europe, mid-latitude North Atlantic, and much of South Asia and the Indian Ocean. Over the "roaring forties" in the Southern Hemisphere, high winds generate a large amount of sea-salt. Such elevation of optical depth, along with high solar zenith angle and hence large backscattering to space, results in a band of TOA cooling of more than -4 Wm^{-2}. Some differences exist between different approaches. For

example, the early post-launch MISR retrieved optical depths over the southern hemisphere oceans are higher than MODIS retrievals and GOCART simulations. Over the "roaring forties", the MODIS derived TOA solar flux perturbations are larger than the estimates from other approaches. The "roaring forties" are a difficult region for remote sensing of aerosol and may be affected by cloud artifacts.

Figure 2.14 shows seasonal and annual mean AOD (first row), clear-sky DRE at the TOA (second row) and surface (third row) derived from averaging the satellite-based estimates and satellite-model integrations (i.e., category A and B in Table 2.4) with an equal weight over 13 regions, ocean and land separately. Correspondingly the probability distribution functions of seasonal and regional DREs are shown in **Figure 2.15**. These figures highlight large seasonal and regional variations of aerosol direct radiative effect. The DRE is relatively narrowly distributed at the TOA and over ocean, compared to that at the surface and over land

Figure 2.16 summarizes the measurement- and model-based estimates of clear-sky annually- averaged DRE at both the TOA and surface from 60°S to 60°N. Seasonal DRE values for individual estimates are summarized in **Table 2.5** (**Box 2.5**) and **Table 2.6** (**Box 2.6**), for ocean and land, respectively. Mean, median and standard error ε ($\varepsilon=\sigma/(n-1)^{1/2}$), where σ is standard deviation and n is the number of methods) are calculated for measurement- and model-based estimates separately. Note that while

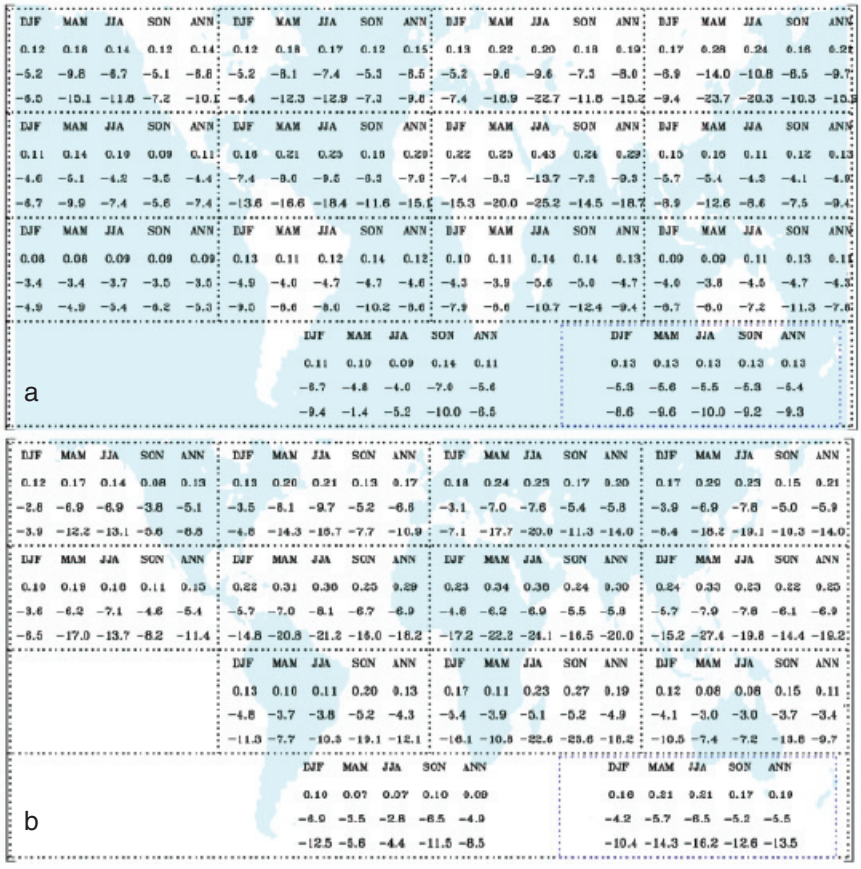

Figure 2.14: Observational-based AOD (first row in each section) and clear-sky DRE (Wm^{-2}) at the TOA (second row) and surface (third row) over 13 oceanic (a) and continental (b) sections (i.e., shadowed areas) derived from equally-weighted average of satellite-based and satellite-model integration-based estimates listed in Table 2. The lower-right boxes are for global oceanic and continental averages, respectively.

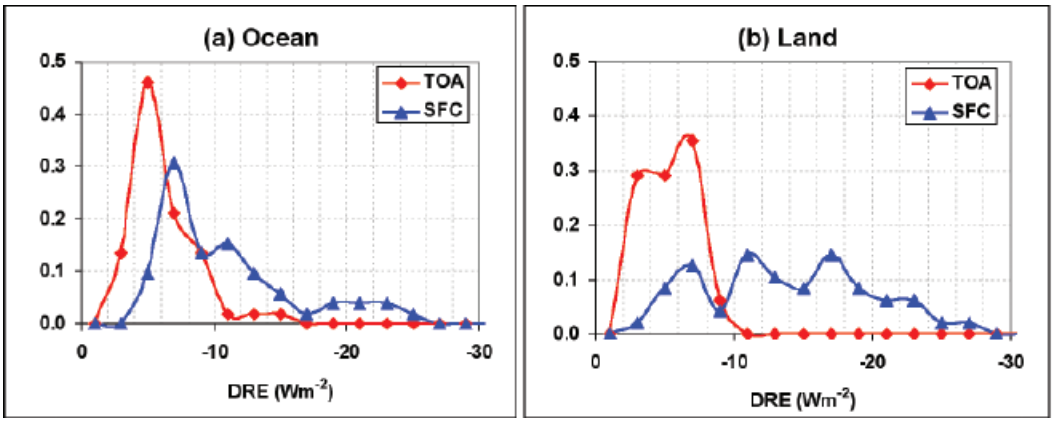

Figure 2.15: Frequency distribution of seasonal and regional average DRE for (a) Ocean and (b) Land, based on sectional and seasonal average data shown in Figure 2.14.

the standard deviation or standard error reported here is not a fully rigorous measure of a true experimental uncertainty, it is indicative of the uncertainty because independent approaches with independent sources of errors are used (see Table 2.4).

For the aerosol direct effect at the TOA and over ocean, a majority of measurement-based and satellite-model integration-based estimates agree with each other within about 10%. On annual average, the measurement-based estimates give the DRE of -5.5±0.2 Wm^{-2} (median±ε) at the TOA and -8.8±0.7 Wm^{-2} at the surface. This suggests that the ocean surface cooling is about 60% larger than the cooling at the TOA.

Model simulations give wide ranges of DRE estimates at both the TOA and surface. The ensemble of five models gives the annual average DRE (median ± ε) of -3.5±0.6 Wm^{-2} and -4.8±0.8 Wm^{-2} at the TOA and surface, respectively. On average, the surface cooling is about 37% larger than the TOA cooling, smaller than the measurement-based estimate of surface and TOA difference of 60%. Large DRE differences between models result from a combination of differences in parameterizations of various aerosol processes and meteorological fields, which are documented under the AEROCOM and Global Modeling Initiative (GMI) frameworks (Kinne et al., 2006; Textor et al., 2006; Liu et al., 2007).

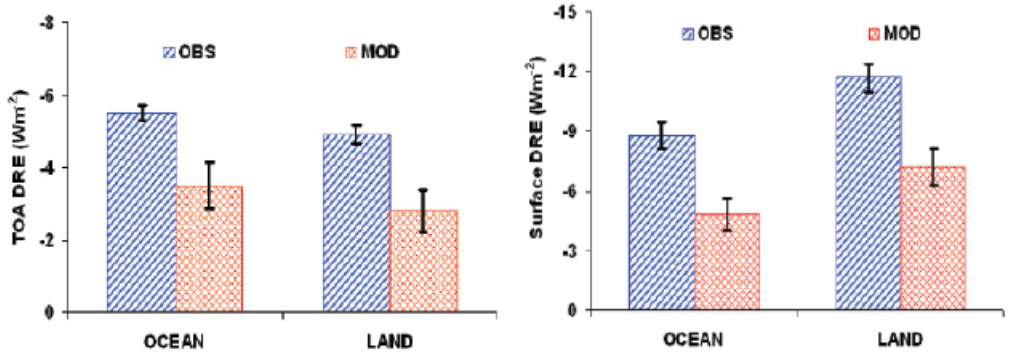

Figure 2.16: Summary of observation- and model-based (denoted as OBS and MOD, respectively) estimates of clear-sky, annual average DRE at the TOA and at the surface. The box and vertical bar represent median and standard error, respectively. (taken from Yu et al., 2006)

Box 2.5 (Table 2.5): Summary of seasonal and annual average clear-sky DRE (Wm^{-2}) at the TOA and the surface (SFC) over global OCEAN derived with different methods and data.

Sources of data: MODIS (Remer & Kaufman, 2006), MODIS_A (Bellouin et al., 2005), POLDER (Boucher and Tanré, 2000; Bellouin et al., 2003), CERES_A and CERES_B (Loeb and Manalo-Smith, 2005), CERES_C (Zhang et al., 2005b), MODIS_G, MISR_G, MO_GO, MO_MI_GO (Yu et al., 2004; 2006), SeaWiFS (Chou et al., 2002), GOCART (Chin et al., 2002; Yu et al., 2004), SPRINTARS (Takemura et al., 2002), GISS (Koch and Hansen, 2005; Koch et al., 2006), LMDZ-INCA (Kinne et al., 2006; Schulz et al., 2006), LMDZ-LOA (Reddy et al., 2005a, b). Mean, median, standard deviation (σ), and standard error (ε) are calculated for observations (Obs) and model simulations (Mod) separately. The last row is the ratio of model median to observational median. (taken from Yu et al., 2006)

Products	DJF		MAM		JJA		SON		ANN	
	TOA	SFC	TOA	SFC	TOA	SFC	TOA	SFC	TOA	SFC
MODIS	-5.9	–	-5.8	–	-6.0	–	-5.8	–	-5.9	–
MODIS_A *	-6.0	-8.2	-6.4	-8.9	-6.5	-9.3	-6.4	-8.9	-6.4	-8.9
CERES_A	-5.2	–	-6.1	–	-5.4	–	-5.1	–	-5.5	–
CERES_B	-3.8	–	-4.3	–	-3.5	–	-3.6	–	-3.8	–
CERES_C	-5.3	–	-5.4	–	-5.2	–	–	–	-5.3	–
MODIS_G	-5.5	-9.1	-5.7	-10.4	-6.0	-10.6	-5.5	-9.8	-5.7	-10.0
MISR_G **	-6.4	-10.3	-6.5	-11.4	-7.0	-11.9	-6.3	-10.9	-6.5	-11.1
MO_GO	-4.9	-7.8	-5.1	-9.3	-5.4	-9.4	-5.0	-8.7	-5.1	-8.8
MO_MI_GO	-4.9	-7.9	-5.1	-9.2	-5.5	-9.5	-5.0	-8.6	-5.1	-8.7
POLDER	-5.7	–	-5.7	–	-5.8	–	-5.6	–	-5.7 -5.2***	-7.7***
SeaWiFS	-6.0	-6.6	-5.2	-5.8	-4.9	-5.6	-5.3	-5.7	-5.4	-5.9
Obs. Mean	-5.4	-8.3	-5.6	-9.2	-5.6	-9.4	-5.4	-8.8	-5.5	-8.7
Obs. Median	-5.5	-8.1	-5.7	-9.3	-5.5	-9.5	-5.4	-8.8	-5.5	-8.8
Obs. σ	0.72	1.26	0.64	1.89	0.91	2.10	0.79	1.74	0.70	1.65
Obs. ε	0.23	0.56	0.20	0.85	0.29	0.94	0.26	0.78	0.21	0.67
GOCART	-3.6	-5.7	-4.0	-7.2	-4.7	-8.0	-4.0	-6.8	-4.1	-6.9
SPRINTARS	-1.5	-2.5	-1.5	-2.5	-1.9	-3.3	-1.5	-2.5	-1.6	-2.7
GISS	-3.3	-4.1	-3.5	-4.6	-3.5	-4.9	-3.8	-5.4	-3.5	-4.8
LMDZ -INCA	-4.6	-5.6	-4.7	-5.9	-5.0	-6.3	-4.8	-5.5	-4.7	-5.8
LMDZ -LOA	-2.2	-4.1	-2.2	-3.7	-2.5	-4.4	-2.2	-4.1	-2.3	-4.1
Mod. Mean	-3.0	-4.4	-3.2	-4.8	-3.5	-5.4	-3.3	-4.9	-3.2	-4.9
Mod. Median	-3.3	-4.1	-3.5	-4.6	-3.5	-4.9	-3.8	-5.4	-3.5	-4.8
Mod. σ	1.21	1.32	1.31	1.84	1.35	1.82	1.36	1.63	1.28	1.6
Mod. ε	0.61	0.66	0.66	0.92	0.67	0.91	0.68	0.81	0.64	0.80
Mod./Obs.	0.60	0.51	0.61	0.50	0.64	0.52	0.70	0.61	0.64	0.55

* High bias may result from adding the DRE of individual components to derive the total DRE (Bellouin et al., 2005).

** High bias most likely results from an overall overestimate of 20% in early post-launch MISR optical depth retrievals (Kahn et al., 2005).

*** Bellouin et al. (2003) use AERONET retrieval of aerosol absorption as a constraint to the method in Boucher and Tanré (2000), deriving aerosol direct effects both at the TOA and the surface.

Box 2.6 (Table 2.6): Summary of seasonal and annual average clear-sky DRE (Wm^{-2}) at the TOA and the surface over global LAND derived with different methods and data.

Sources of data: MODIS_G, MISR_G, MO_GO, MO_MI_GO (Yu et al., 2004, 2006), GOCART (Chin et al., 2002; Yu et al., 2004), SPRINTARS (Takemura et al., 2002), GISS (Koch and Hansen, 2005; Koch et al., 2006), LMDZ-INCA (Balkanski et al., 2007; Kinne et al., 2006; Schulz et al., 2006), LMDZ-LOA (Reddy et al., 2005a, b). Mean, median, standard deviation (σ), and standard error (ε) are calculated for observations (Obs) and model simulations (Mod) separately. The last row is the ratio of model median to observational median. (taken from Yu et al., 2006)

Products	DJF		MAM		JJA		SON		ANN	
	TOA	SFC	TOA	SFC	TOA	SFC	TOA	SFC	TOA	SFC
MODIS_G	-4.1	-9.1	-5.8	-14.9	-6.6	-17.4	-5.4	-12.8	-5.5	-13.5
MISR_G	-3.9	-8.7	-5.1	-13.0	-5.8	-14.6	-4.6	-10.7	-4.9	-11.8
MO_GO	-3.5	-7.5	-5.1	-12.9	-5.8	-14.9	-4.8	-10.9	-4.8	-11.6
MO_MI_GO	-3.4	-7.4	-4.7	-11.8	-5.3	-13.5	-4.3	-9.7	-4.4	-10.6
Obs. Mean	-3.7	-8.2	-5.2	-13.2	-5.9	-15.1	-4.8	-11.0	-4.9	-11.9
Obs. Median	-3.7	-8.1	-5.1	-13.0	-5.8	-14.8	-4.7	-10.8	-4.9	-11.7
Obs. σ	0.33	0.85	0.46	1.29	0.54	1.65	0.46	1.29	0.45	1.20
Obs. ε	0.17	0.49	0.26	0.74	0.31	0.85	0.27	0.75	0.26	0.70
GOCART	-2.9	-6.1	-4.4	-10.9	-4.8	-12.3	-4.3	-9.3	-4.1	-9.7
SPRINTARS	-1.4	-4.0	-1.5	-4.6	-2.0	-6.7	-1.7	-5.2	-1.7	-5.1
GISS	-1.6	-3.9	-3.2	-7.9	-3.6	-9.3	-2.5	-6.6	-2.8	-7.2
LMDZ-INCA	-3.0	-5.8	-4.0	-9.2	-6.0	-13.5	-4.3	-8.2	-4.3	-9.2
LMDZ-LOA	-1.3	-5.4	-1.8	-6.4	-2.7	-8.9	-2.1	-6.7	-2.0	-6.9
Mod. Mean	-2.0	-5.0	-3.0	-7.8	-3.8	-10.1	-3.0	-7.2	-3.0	-7.6
Mod. Median	-1.6	-5.4	-3.2	-7.9	-3.6	-9.3	-2.5	-6.7	-2.8	-7.2
Mod. σ	0.84	1.03	1.29	2.44	1.61	2.74	1.24	1.58	1.19	1.86
Mod. ε	0.42	0.51	0.65	1.22	0.80	1.37	0.62	0.79	0.59	0.93
Mod./Obs.	0.43	0.67	0.63	0.61	0.62	0.63	0.53	0.62	0.58	0.62

Clearly the model-based ensemble estimates of DRE are 30-50% smaller than the measurement-based estimates. As discussed earlier, MODIS retrieved optical depths tend to be overestimated by about 10-15% due to the contamination of thin cirrus and clouds in general (Kaufman et al., 2005b). Such overestimation of optical depth would result in a comparable overestimate of the aerosol direct radiative effect. Other satellite AOD data may have similar contamination, which however has not yet been quantified. For simplicity, we assume a cloud contamination of 10-15% in the measurement-based average DRE. With this correction of cloud contamination, the discrepancy between the measurement-based and model-based estimates of DRE and radiative efficiency would be reduced to 15-40%. On the other hand, the observations may be measuring enhanced AOD and DRE due to processes not well represented in the models including humidification and enhancement of aerosols in the vicinity of

clouds (Koren et al., 2007a). From the perspective of model simulations, uncertainties associated with a number of factors will contribute to the measurement-model discrepancy. Factors determining the AOD should be major reasons for the DRE discrepancy and the constraint of model AOD with well evaluated and bias reduced satellite AOD through a data assimilation approach can reduce the DRE discrepancy significantly. Other factors (such as model parameterization of surface reflectance, and model-satellite differences in single-scattering albedo and asymmetry factor due to satellite sampling bias toward cloud-free conditions) should also contribute, as evidenced by the existence of a large discrepancy in the radiative efficiency (Yu et al., 2006). Significant endeavor is demanded in the future to conduct comprehensive assessments.

Currently, satellite measurements alone are not adequate to characterize complex aerosol properties over complex surfaces and hence can not be used to derive the aerosol direct effect over land with high accuracy. As such, DRE estimates over land have to rely on model simulations and satellite-model integrations. On a global and annual average, the satellite-model integrated approaches derive a median DRE of -4.9 Wm^{-2} at the TOA and -11.7 Wm^{-2} at the surface respectively. The surface cooling is about 2.4 times larger than the TOA cooling because of aerosol absorption.

An ensemble of five model simulations derives a DRE (median ± ε) over land of -2.8±0.6 Wm^{-2} at the TOA and -7.2±0.9 Wm^{-2} at the surface, respectively. These are about 40% smaller than the measurement-based estimates. The measurement-model differences are a combination of differences in aerosol amount (optical depth), single-scattering properties, surface albedo, and radiative transfer schemes (Yu et al., 2006). Seasonal variations of DRE over land, as derived from both measurements and models, are larger than those over ocean.

2.3.4. *Satellite Based Estimates of Anthropogenic Aerosol Direct Climate Forcing*

Satellite instruments do not measure the aerosol chemical composition needed to discriminate anthropogenic from natural aerosol components. Because anthropogenic aerosols are predominately submicron, the fine-mode fraction derived from POLDER, MODIS, or MISR might be used as a tool for deriving anthropogenic aerosol optical depth. This could provide a feasible way to conduct measurement-based estimates of anthropogenic aerosol forcing (Kaufman et al., 2002a). The MODIS-based estimate of anthropogenic AOD is about 0.033 over oceans, consistent with model assessments of 0.03~0.036 even though the total AOD from MODIS is 25-40% higher than the models (Kaufman et al., 2005a). This accounts for 21±7% of the MODIS-observed total aerosol optical depth, compared with about 33% of anthropogenic contributions estimated by the models. The anthropogenic fraction of AOD should be much larger over land (i.e., 47±9% from a composite of several models) (Bellouin et al., 2005), comparable to the 40% estimated by Yu et al. (2006). Similarly, the non-spherical fraction from MISR or POLDER could also be used to separate dust from anthropogenic aerosol (Kahn et al., 2001).

In Kaufman et al. (2005a), it was assumed that all biomass burning aerosol is anthropogenic and all dust aerosol is natural. The better determination of anthropogenic aerosols requires a quantification of biomass burning ignited by lightning (natural origin) and mineral dust due to human induced changes of land cover/land use and climate (anthropogenic origin), which remains uncertain. Recent modeling (Tegen et al., 2004) suggests that the anthropogenic sources of dust contribute less than 10% of the

Table 2.7: Estimates of anthropogenic aerosol optical depth (τant) and clear-sky DCF at the TOA from model simulations (Schulz et al., 2006) and approaches constrained by satellite observations (Kaufman et al., 2005; Bellouin et al., 2005, 2008; Chung et al., 2005; Yu et al., 2006; Christopher et al., 2006; Matsui and Pielke, 2006; Quaas et al., 2008; Zhao et al., 2008).

Data Sources	Ocean		Land		Global		Estimated uncertainty or model diversity for DCF
	τ_{ant}	DCF (Wm^{-2})	τ_{ant}	DCF (Wm^{-2})	τ_{ant}	DCF (Wm^{-2})	
Kaufman et al. (2005)	0.033	-1.4	-	-	-	-	30%
Bellouin et al. (2005)	0.028	-0.8	0.13	-	0.062	-1.9	15%
Chung et al. (2005)	-	-	-	-	-	-1.1	-
Yu et al. (2006)	0.031	-1.1	0.088	-1.8	0.048	-1.3	47% (ocean), 84% (land), and 62% (global)
Christopher et al. (2006)	-	-1.4	-	-	-	-	65%
Matsui and Pielke (2006)	-	-1.6	-	-	-	-	30°S-30°N oceans
Quaas et al. (2008)	-	-0.7	-	-1.8	-	-0.9	45%
Bellouin et al. (2008)	0.021	-0.6	0.107	-3.3	0.043	-1.3	Update to Bellouin et al. (2005) with MODIS Collection 5 data
Zhao et al. (2008)	-	-1.25	-	-	-	-	35%
Schulz et al. (2006)	0.022	-0.59	0.065	-1.14	0.036	-0.77	30-40%; same emissions prescribed for all models

total dust optical depth, although early studies speculated the fraction to be between 0% (Ginoux et al., 2001) and 50% (Tegen and Fung, 1995).

To improve satellite estimates of anthropogenic aerosols and their direct forcing, satellite programs should concentrate on validating and improving retrievals of the aerosol Ångström exponent, and suborbital measurements should be used to derive relationships between the Ångström exponent and fine-mode fraction to allow interpretation of the satellite derived fine-mode optical depth (Anderson et al., 2005b).

There have been several estimates of DCF by anthropogenic aerosols in recent years. **Table 2.7** lists such estimates of TOA DCF that are from model simulations (Schulz et al., 2006) and constrained to some degree by satellite observations (Kaufman et al., 2005a; Bellouin et al., 2005, 2008; Chung et al., 2005; Christopher et al., 2006; Matsui and Pielke, 2006; Yu et al., 2006; Quaas et al.,2008; Zhao et al., 2008). The satellite-based clear-sky DCF by anthropogenic aerosols is estimated to be -1.1 ± 0.37 Wm^{-2} over ocean, about a factor of 2 stronger than model simulated -0.6 Wm^{-2}. Similar DCF estimates are rare over land, but a few studies do suggest that the DCF over land is much more negative than that over ocean (Yu et al., 2006; Bellouin et al., 2005, 2008). On global average, the measurement-based estimate of DCF ranges from -0.9~-1.9 Wm^{-2}, again stronger than the model-based estimate of -0.8 Wm^{-2}. Similar to DRE estimates, satellite-based DCF estimates are rare over land. DCF estimates have larger uncertainty than DRE estimates, particularly over land.

An uncertainty analysis (Yu et al., 2006) partitions the uncertainty for the global average DCF between land and ocean more or less evenly. Five parameters, namely fine-mode fraction (f_f) and anthropogenic fraction of fine-mode fraction (f_{af}) over both land and ocean, and τ over ocean, contribute nearly 80%

of the overall uncertainty in the DCF estimate, with individual shares ranging from 13-20% (Yu et al., 2006). We should point out that these uncertainties presumably represent a lower bound because the sources of error are assumed to be independent. Uncertainties associated with several parameters are also not well defined. Nevertheless, such uncertainty analysis is useful for guiding future research and documenting advances in our understanding.

On global average, anthropogenic aerosols are generally more absorptive than natural aerosols. As such the surface DCF is much more negative than the TOA DCF. Several observation-constrained studies estimate the global average clear-sky DCF at the surface of -4.2 ~ -5.1Wm^{-2} (Yu et al., 2004; Bellouin et al., 2005; Chung et al., 2005; Matsui and Pielke, 2006), which is about a factor of 2 larger in magnitude than the model estimates (e.g., Reddy et al., 2005b).

2.3.5. *Remote Sensing Studies of Aerosol-Cloud Interactions and Indirect Effects*

Satellite views of the Earth inevitably show a planet covered, not by aerosols, but by clouds. The bright white clouds overlying darker oceans or vegetated surface demonstrate the significant effect that clouds have on the Earth's radiative balance. Low clouds reflect incoming sunlight back to space, acting to cool the planet, while high clouds can trap outgoing terrestrial radiation and act to warm the planet. Changes in cloud cover, in cloud vertical development, and cloud optical properties will have strong radiative and therefore, climatic impacts. Furthermore, factors that change cloud development will also change precipitation processes. These changes can alter amounts, locations and intensities of local and regional rain and snowfall, creating droughts, floods and severe weather.

Aerosol particles act as cloud condensation nuclei (*CCN*). Every cloud droplet consists of water condensing onto one or more of these CCN. Thus, for the same amount of liquid water in a cloud, more available CCN will result in a greater number but smaller size of droplets (Twomey, 1977). A cloud with smaller but more numerous droplets will be brighter and reflect more sunlight to space. This is the aerosol indirect radiative effect. However, because the droplets are smaller they may inhibit collision-coalescence in the cloud, suppressing particle growth that stops drizzle and other precipitation and extends cloud lifetime (Albrecht et al. 1989). In a cloud with strong updrafts, the cloud may eventually precipitate, but only after higher altitudes are reached that result in taller cloud tops, more lightning and greater chance of severe weather (Rosenfeld and Lensky, 1998; Andreae et al., 2004).

On the other hand, because aerosols themselves are radiatively active, they can change atmospheric conditions (temperature, stability) that also influences cloud development and properties (Hansen et al, 1997; Ackerman et al., 2000). Thus, aerosols affect clouds both through changing cloud droplet size distributions, and by changing the atmospheric environment of the cloud.

The AVHRR satellites have observed relationships between columnar aerosol loading and retrieved cloud microphysics and cloud brightness over the Amazon Basin that are consistent with the theories explained above (Kaufman and Nakajima, 1993; Kaufman and Fraser, 1997; Feingold et al., 2001). Other studies have linked cloud and aerosol microphysical parameters or cloud albedo and droplet size using satellite data applied over the entire global oceans (Wetzel and Stowe, 1999; Nakajima et al., 2001; Han et al., 1998). Using these correlations with estimates of aerosol increase from the pre-industrial era, estimates of anthropogenic aerosol indirect radiative forcing fall into the range of -0.7 to -1.7 Wm^{-2} (Nakajima et al., 2001).

Introduction of the more modern instruments (POLDER and MODIS) have allowed more detailed observations of relationships between aerosol and cloud parameters. Cloud cover can both decrease and increase with increasing aerosol loading (Koren et al., 2004; Kaufman et al., 2005; Koren et al., 2005; Sekiguchi et al., 2003; Yu et al., 2007). Aerosol absorption appears to be an important factor in determining how cloud cover will respond to increased aerosol (Kaufman and Koren, 2006; Jiang and Feingold, 2006). Different responses of cloud cover to increased aerosol could also be correlated with atmospheric thermodynamic and moisture structure (Yu et al., 2007). Observations in the MODIS data show that aerosol loading correlates with enhanced convection and greater production of ice anvils in the summer Atlantic Ocean (Koren et al., 2005), which conflicts with previous results that used AVHRR and could not isolate convective systems from shallow clouds (Sekiguchi et al., 2003).

In recent years, surface-based remote sensing has also been applied to address aerosol effects on cloud microphysics. This method offers some interesting insights, and is complementary to the global satellite view. Surface remote sensing can only be applied at a limited number of locations, and therefore lacks the global satellite view. However, these surface stations yield high temporal resolution data and because they sample aerosol below, rather than adjacent to clouds they do not suffer from "cloud contamination". With the appropriate instrumentation (lidar) they can measure the local aerosol entering the clouds, rather than a column-integrated aerosol optical depth.

Feingold et al. (2003) used data collected at the Atmospheric Radiation Measurement (*ARM*) site to allow simultaneous retrieval of aerosol and cloud properties, with the combination of a Doppler cloud radar and a microwave radiometer to retrieve cloud drop effective radius r_e profiles in non-precipitating (radar reflectivity Z < -17 dBZ), ice-free clouds. Simultaneously, sub-cloud aerosol extinction profiles were measured with a lidar to quantify the response of drop sizes to changes in aerosol properties. The microwave radiometer made it possible to sort the cloud data according to liquid water path (*LWP*), consistent with Twomey's (1977) conceptual view of the aerosol impact on cloud microphysics. With high temporal/spatial resolution data (on the order of 20's or 100's of meters), realizations of aerosol-cloud interactions at the large eddy scale were obtained. Moreover, by examining updrafts only (using the radar Doppler signal), the role of updraft in determining the response of r_e to changes in aerosol (via changes in drop number concentration N_d) was examined. Analysis of data from 7 days showed that turbulence intensifies the aerosol impact on cloud microphysics.

In addition to radar/microwave radiometer retrievals of aerosol and cloud properties, surface based radiometers such as the MFRSR (Michalsky et al., 2001) have been used in combination with a microwave radiometer to measure an average value of r_e during daylight when the solar elevation angle is sufficiently high (Min and Harrison, 1996). Using this retrieval, Kim et al. (2003) performed analyses of the r_e response to changes in aerosol at the same continental site, and instead of using extinction as a proxy for CCN, they used a surface measurement of the aerosol light scattering coefficient. Their analysis spanned much longer time periods and their data included a range of different aerosol conditions. A similar study was conducted by Garrett et al. (2004) at a location in the Arctic. The advantage of the MFRSR/microwave radiometer combination is that it derives r_e from cloud optical depth and LWP and it is not sensitive to large drops as the radar is. Its drawback is that it can only be applied to clouds with extensive horizontal cover during daylight hours.

In conclusion, observational estimates of aerosol indirect radiative effects are still in their infancy. Effects on cloud microphysics that result in cloud brightening have to be balanced by effects on cloud

lifetime, cover, vertical development and ice production. Aerosol type and specifically the absorption properties of the aerosol may cause different cloud responses. Early estimates of observationally based aerosol indirect forcing range from -0.7 to -1.7 Wm^{-2} (Nakajima et al, 2001) and -0.6 to -1.2 Wm^{-2} (Sekiguchi et al., 2003), depending on the estimate for aerosol increase from pre-industrial times and whether aerosol effects on cloud fraction are also included in the estimate.

2.4. Outstanding Issues

Despite substantial progress in the assessment of the aerosol radiative effect and forcing as summarized in section 2.2 and 2.3, several important issues remain, and significant efforts are required to address them.

2.4.1. *Aerosol Vertical Distributions*

Vertical distributions of aerosols are crucial to quantifying the aerosol direct effect in the thermal infrared and in cloudy conditions, interpreting the satellite observed aerosol-cloud correlations, and understanding the atmospheric response to aerosol radiative forcing.

Due to its large size, mineral dust can cause warming in the thermal infrared, both at the TOA and at the surface. Therefore, estimates of aerosol direct effect on solar radiation should represent an upper bound of the aerosol net direct effect (on total radiative fluxes). The warming effect could be significant, as suggested by a few observational studies (Highwood et al., 2003; Haywood et al., 2005; Zhang and Christopher, 2003; Slingo et al., 2006). However, current estimates of the warming effects in the thermal infrared remain highly uncertain, because of lack of observations of vertical distributions of aerosol in the thermal infrared range (Sokolik et al., 2001; Lubin et al., 2002). In addition, the scattering effect in the thermal infrared domain is generally neglected in most GCMs, which may lead to an underestimate of the thermal infrared aerosol effect (Dufresne et al., 2002).

Calculations of the cloudy-sky aerosol direct effect require an adequate characterization of vertical distributions of aerosols and three-dimensional fields of clouds, especially for absorbing aerosols. The surface cooling in climatologically cloudy conditions is comparable to that under clear conditions, while the TOA effect could switch from cooling in clear conditions to warming in overcast conditions (Keil and Haywood, 2003). Note that substantial differences currently exist in simulations of aerosol vertical distributions (Penner et al., 2002; Textor et al., 2006) and limited measurements do not suffice for the estimate of the cloudy-sky DRE and DCF. This is manifested by a large diversity in the calculated whole-sky to clear-sky ratio for the TOA DCF (Schulz et al., 2006; Chung et al., 2005; Reddy and Boucher, 2004; Takemura et al., 2001; Jacobson, 2001), as summarized in **Figure 2.17**. The ratio ranges from +0.5 to -0.1 (i.e., shifting from clear-sky cooling to whole-sky warming), with an average of 0.26, and standard deviation of 0.17.

The emerging ground-based aerosol lidar networks and spaceborne lidars and radars (Stephens et al., 2001) will help improve the understanding of the aerosol direct forcing in cloudy conditions and the thermal infrared range. The lidar measurements can also well constrain the aerosol-induced atmospheric heating rate increment that is essential for assessing atmospheric responses to the aerosol radiative forcing (e.g., Yu et al., 2002; Feingold et al., 2005; Lau et al., 2006).

2.4.2. *Aerosol Direct Forcing over Land*

The land surface reflection is large, heterogeneous, and anisotropic, which complicates aerosol retrievals and determination of the aerosol direct effect. For example, the lack of a dust signal over the deserts (Hsu et al., 2000) is apparently attributable to the large heterogeneity of surface reflectance as documented by high-resolution MODIS land albedo retrievals (Tsvetsinskaya et al., 2002). The current-generation satellite sensors like MODIS and MISR are improving the characterization of land surface reflection by measuring its wavelength dependence and angular distribution at high resolution. This offers a promising opportunity for inferring the aerosol direct effect over land from satellite measurements of radiative fluxes (e.g., CERES) and from critical reflectance techniques (Fraser and Kaufman, 1985; Kaufman, 1987). Such satellite-based estimates should be comprehensively evaluated against those calculated from AERONET measurements (Zhou et al., 2005) and intensive field experiments (as summarized in Yu et al., 2006).

2.4.3. *Aerosol Absorption*

Aerosol absorption and single-scattering albedo are strong functions of the size of particles, the state of mixture, the shape, the wavelength and the relative humidity. A characterization of aerosol absorption or SSA is complicated by instrumental errors and modeling inadequacies, as summarized in Heintzenberg et al. (1997), Reid et al. (2005), and Bond and Bergstrom (2006). The global assessment of aerosol absorption and SSA represents a major challenge in efforts to quantify the direct forcing (Yu et al., 2006) and aerosol-cloud interactions (Kaufman and Koren, 2006).

Instrument calibration for aerosol absorption measurements is challenging, because aerosol absorption typically has a much smaller magnitude than aerosol scattering (Heintzenberg et al., 1997; Bond and Bergstrom, 2006). Determining aerosol absorption by subtracting measured scattering from measured

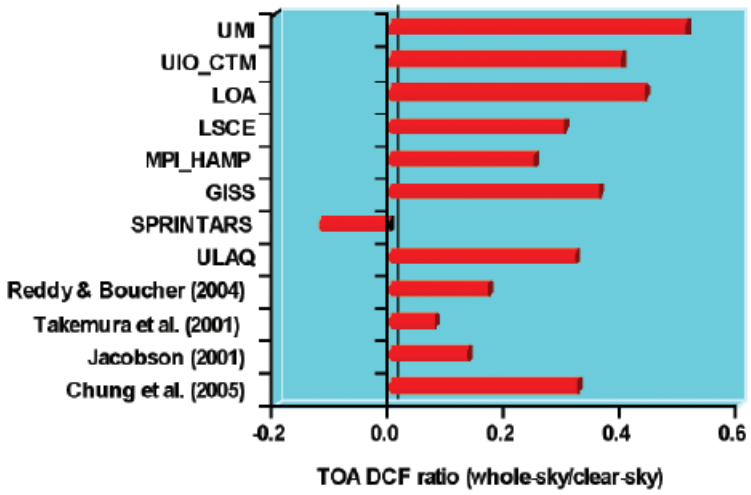

Figure 2.17: Summary of model-based estimates of whole-sky to clear-sky ratio for the TOA DCF. Model simulations are taken from Schulz et al. (2006), except otherwise specified.

extinction could have large uncertainties. Recent employment of photoacoustic methods (Arnott et al., 1997) and cavity ring down extinction cells (Strawa et al., 2002) will significantly improve the accuracy of SSA measurement. In-situ measurements are generally conducted at low relative humidity and effects of water uptake on aerosol absorption are poorly understood (Redemman et al., 2001).

Model simulations of aerosol compositions have large diversities, as shown in **Figure 2.11**. It is necessary to constrain model simulations with optical models consistent with in-situ measurements of aerosol physical and optical properties (Bond and Bergstrom, 2006). While nonabsorbing aerosols don't directly contribute to aerosol absorption, it is necessary to better characterize the evolution of nonabsorbing aerosols such as hydrophilic sulfate and their interactions with black carbon (BC) in models (Stier et al., 2006). The mixing of sulfate and BC can turn initially hydrophobic BC to a hydrophilic state and hence enhance removal by wet scavenging and decrease BC abundance and absorption. In addition, the presence of sulfate also can increase the BC absorption efficiency through internal mixing and increasing the amount of diffuse solar radiation. The first mechanism prevails in remote regions, reducing aerosol absorption. Near source regions, the second mechanism could prevail and hence enhance the solar absorption (Stier et al., 2006).

Inverse methods have been widely used in both ground and satellite remote sensing, providing aerosol absorption information over large geographical areas and during long time periods. The theoretical uncertainty of the AERONET retrieval of SSA is 0.03 for AOD greater than 0.3 (Dubovik et al., 2002). Similarly, at large AOD the estimated AERONET uncertainty for absorptive optical depth is 0.01 (Dubovik and King, 2000; Dubovik et al., 2001). It is important to pursue validation against independent measurements because a recent study has shown a factor of 2-4 discrepancy between the AERONET retrievals and the simulated absorptive optical depths (Sato et al., 2003). This discrepancy would imply significant errors in the global burden of black carbon and/or the absorptive efficiency of black carbon (perhaps related to aerosol mixing state, morphology, or size distribution) (Sato et al., 2003; Martins et al., 1998; Jacobson, 2000; 2001). On the other hand, a comparison of in-situ to AERONET absorption over the Chesapeake Bay indicated that the latter may be biased high (Magi et al., 2005). AERONET Version 2 retrievals of aerosol SSA are expected to be more accurate due to improved characterization of seasonal, spectral, and BRDF of surface reflection and the SSA retrievals over bright surfaces are substantially lower than that in Version 1 (Leahy et al., 2007). This warrants a reexamination of discrepancies/agreements between AERONET retrievals and in-situ measurements (Haywood et al., 2003; Magi et al., 2005). It is essential to pursue a better understanding of the uncertainty of in-situ measured and remote sensing inversed SSA in a robust way and accordingly a synthesis of different data sets for yielding regional characterization of aerosol absorption with well-defined uncertainty (Leahy et al., 2007).

Satellite methods for quantifying SSA and absorption have been developed and partially validated at UV wavelengths (Torres et al., 2005), although the retrieval has large uncertainties associated with its sensitivity to the height of the aerosol layer and it is unclear at present how these UV results can be extended to visible wavelengths. Examining satellite images in dusty conditions (Kaufman et al., 2001; Moulin et al., 2001) suggests that mineral dust absorption could be much weaker than previously believed (e.g., Patterson et al., 1977) and widely used in model simulations, corroborated by in-situ and ground-based remote sensing measurements (e.g., Clarke and Charlson, 1985; Dubovik et al., 2002; Cattrall et al., 2003; Haywood et al., 2003). This finding could partly explain the measurement-model

discrepancies in aerosol direct radiative effect (e.g., Yu et al., 2004). It is thus important to reevaluate and improve model simulations of mineral dust aerosol radiative effect by explicitly accounting for the dependence on mineralogy and morphology of dust (Sokolik and Toon, 1999; Sokolik et al., 2001; Balkanski et al., 2007). Views in and out of sunglint can be used to retrieve total aerosol extinction and scattering, respectively, thus constraining aerosol absorption over oceans (Kaufman et al., 2002b). However, the technique requires highly accurate retrievals of aerosol scattering properties including the real part of the refractive index. Only a polarization instrument can provide that information. The technique will be applied to the collocated MODIS and PARASOL data in the A-Train. The technique will also be applied to APS data from the Glory mission.

2.4.4. *Diurnal Cycle*

Significant efforts are demanded to capture the diurnal cycle of aerosol direct forcing in order to better assess aerosol impacts on climate. AERONET measurements show that the daytime variability depends on location and aerosol type, with the variation as large as 40% for biomass burning smoke and urban/industrial pollution near the sources, and essentially negligible for dust (Smirnov et al., 2002). From the perspective of satellite remote sensing, the diurnal variation of aerosols can be better characterized by geostationary satellites (*GOES*) (Christopher and Zhang, 2002b; Wang et al., 2003). However, these satellites generally lack the information required to characterize aerosol types. The synergistic use of low earth orbit (for characterizing aerosol type) and geostationary earth orbit satellite data should be used to retrieve aerosol optical depth and its diurnal variations (Costa et al., 2004a, 2004b). MODIS flying on the twin EOS satellites, namely Terra and Aqua, can also be used to some extent to examine aerosol diurnal variations, i.e., from late morning (10:30 LT) to early afternoon (13:30 LT) (Remer et al., 2006; Ichoku et al., 2005).

Clouds can modulate the aerosol direct solar effect significantly and daytime variation of clouds needs to be adequately characterized. The aerosol direct effect also depends on surface reflection, and the anisotropy of surface reflection further complicates the calculation of the diurnal cycle of the aerosol radiative effect (Yu et al., 2004). With satellite remote sensing providing angular and spectral variations of surface reflection (e.g., Moody et al., 2005; Martonchik et al., 1998; 2002), it is feasible to better characterize the complexity of surface reflection and its interaction with aerosol extinction through the use of the black-sky and white-sky albedo for direct beam and diffuse light, respectively (Yu et al., 2004, 2006).

2.4.5. *Aerosol-Cloud Interactions and Indirect Forcing*

Remote sensing estimates of aerosol indirect forcing are still rare and uncertain. Basic processes still need to be understood on regional and global scales. Uncertainties will likely increase before they decrease as new processes and their feedbacks become known. Remote sensing observations of aerosol-cloud interactions and aerosol indirect forcing are now simple correlations between variables, in which cause-and-effects are inferred. However, such inferences are not proven. The most difficult aspect of inferring aerosol effects on clouds from the observed relationships is separating aerosol effects from meteorological effects when aerosol loading itself is often correlated with the meteorology. While satellite studies provide indispensable information on aerosol-cloud interaction, future work will need to combine satellite observations with in-situ validation and modeling interpretation.

2.4.6. Long-term Trends of Aerosols and Radiative Fluxes

To detect long-term trends of aerosols, satellite retrievals of aerosol optical depth should have high accuracy and a synergy of aerosol products from multiple sensors (historical sensors and modern sensors) to construct as long a record as possible. Historical sensors like TOMS and AVHRR have provided multi-decadal climatology of aerosol optical depth (Torres et al., 2002; Geogdzhayev et al., 2002), which have been used to analyze trends of aerosol optical depths in Asia (e.g., Massie et al., 2004) and over global ocean (Mishchenko et al., 2007b). These products should be extended to a longer period by incorporating data from modern sensors (e.g., MODIS, MISR, OMI, and others). Such extensions should be built upon our understanding and reconciliation of AOD differences among different sensors or platforms (Jeong et al., 2005). A good deal of effort is needed to address this fundamental issue. An emerging 7-year climatology of high quality AOD data from modern sensors, though not as long as records from historic sensors, has been used to examine the interannual variations of aerosol (Koren et al., 2007b) and shall contribute significantly to the study of aerosol trends.

Broadband direct solar radiation is measured at meteorological stations around the world. These long-term observations can be used to derive average aerosol optical depth over the solar spectrum, thus having the potential to detect changing aerosol conditions on a decadal scale (Luo et al., 2001). However such aerosol optical depth retrievals still need to be evaluated using independent measurements from other surface observations, such as AERONET and MFRSR.

Analysis of long-term records of surface solar radiation suggests significant trends during past decades (e.g., Stanhill and Cohen, 2001; Wild et al., 2005; Pinker et al., 2005). While a significant and widespread decline in surface solar radiation occurred up to 1990 (so-called *dimming*), a sustained increase has been observed in the most recent decade. Speculation suggests that such trends result from decadal changes of aerosols and an interplay of aerosol direct and indirect effects (Stanhill and Cohen, 2001; Wild et al., 2005; Streets et al., 2006b; Norris and Wild, 2007). Other studies suggest that the measured changes in surface solar radiation are local, not global in nature (Alpert et al., 2005). However, reliable observations of aerosol trends are needed before these speculations can be proven or disproven. In addition to the aerosol optical depth, we also need to quantify changes in aerosol composition because of changes in industrial practices, environmental regulations, and biomass burning emissions (Novakov et al., 2003; Streets et al., 2004; Streets and Aunan et al., 2005). Such compositional changes will affect the aerosol single-scattering albedo and size distribution, which in turn will affect the surface solar radiation (e.g., Qian et al., 2007). However such data are currently rare and subject to large uncertainties. A better understanding of aerosol-radiation-cloud interactions is badly needed to attribute the observed radiation changes to aerosol changes with less ambiguity.

2.5. Concluding Remarks

Since the concept of aerosol-radiation-climate interactions was first proposed around 1970, substantial progress has been made in determining the mechanisms and magnitudes of these interactions, particularly in the last ten years. Such advancement has greatly benefited from significant improvements in aerosol measurements and increasing sophistication of model simulations. In particular, the establishment of ground-based aerosol networks such as AERONET and the execution of intensive field

experiments in a variety of aerosol regimes have collected invaluable datasets that serve as a baseline for constraining and evaluating satellite retrievals and model simulations. New and enhanced satellite sensors, such as POLDER, MODIS, and MISR, are measuring aerosols on a global scale and with good accuracy. CERES measures broadband solar and thermal infrared fluxes that are used to derive the aerosol direct radiative effect and forcing.

As a result of these improvements, we now have a much improved knowledge of aerosol properties and their interaction with solar radiation on regional and global scale. Intensive field campaigns conducted in major aerosol regimes around the globe and the emerging ground-based aerosol networks have resulted in better characterization of regional aerosol, including its chemical, microphysical, and radiative properties. Uncertainties associated with them can be well understood through conducting closure studies of over-determined data from multiple platforms and instruments. Aerosol closure studies reveal that for submicrometer, spherical (e.g., sulfate, carbonaceous aerosol) meaurements of aerosol optical properties and optical depths agree within 15% and often better. For dust dominated aerosol, measurements of aerosol optical depth disagree by up to 35% between methods, due to inlet collection efficiency and instrumental response difficulties resulting from its larger particle size and non-sphericity. Closure studies on DRE reveal uncertainties of about 25% for sulfate/carbonaceous aerosol and 60% for dust (Bates et al., 2006)

The accumulated comprehensive data sets of regional aerosol properties provide a rigorous "test bed" and strong constraint for satellite retrievals and model simulations of aerosols and their direct radiative effect and climate forcing. In Bates et al. (2006), in-situ measurements from three major aerosol characterization experiments were used to derive optical properties for individual aerosol types (i.e., sulfate/carbonaceous, dust, and sea-salt aerosol) that are of interest in the calculation of aerosol direct radiative effect, including wavelength-dependent mass extinction efficiency, single-scattering albedo, backscatter and asymmetry factor, and humidification factor for aerosol scattering. Such empirically determined aerosol optical properties were then used to constrain calculations of AOD and DRE in two CTM models. The so-constrained AOD and DRE increase by about 30%, compared to calculations based on the *a priori* optical properties.

For all of their advantages, field campaigns are inherently limited by their relatively short duration and small spatial coverage. Satellite remote sensing can augment field campaigns by expanding the temporal and spatial coverage. Surface networks provide high temporal resolution records but also benefit from the expanded spatial resolution provided by satellites. The multi-spectral MODIS measures global distributions of aerosol optical depth (τ) on a daily scale, with high accuracy of $\pm 0.03 \pm 0.05\tau$ over oceans. The annual average τ at 550 nm is about 0.14 over the global oceans. Based on the MODIS fine-mode and background aerosol fraction, about 21% of the 0.l4 is estimated to be contributed by human activities. The multi-angle MISR can evaluate the surface reflectance and retrieve aerosols simultaneously over all kinds of surfaces, including bright deserts. MISR derives an annual average AOD of 0.23 at 550 nm over global land with an uncertainty of ~20% or ±0.05. A combination of MODIS over-ocean and MISR over-land retrievals gives a global average of aerosol optical depth of about 0.17 at 550 nm, which is 20% larger than an ensemble average of 0.14 of five global aerosol models. It is possible that such discrepancy can be largely reduced by correcting cloud artifacts in satellite retrievals, and by including complex cloud-aerosol physical processes in models.

The high-accuracy of MODIS and MISR aerosol products and broadband flux measurements from CERES, together with simultaneous improvements in surface and cloud characterizations in these sensors, make it feasible to obtain observational constraints for the aerosol direct effect. A number of measurement-based approaches consistently estimate the cloud-free DRE (on solar radiation) at the top-of-atmosphere to be about -5.5±0.2 Wm^{-2} (median ± standard error from various methods) over global ocean. At the ocean surface, the DRE is estimated to be -8.8±0.7 Wm^{-2}. Over land, deriving the aerosol direct effect from the flux measurements such as that from CERES is complicated by a large and highly heterogeneous surface reflection. An integration of satellite retrievals and model simulations yields a DRE of -4.9±0.7 Wm^{-2} and -11.8±1.9 Wm^{-2} at the TOA and surface, respectively. Overall, in comparison to that over ocean, the DRE estimates over land are more poorly constrained by observations and have larger uncertainties. At regional scales, differences between measurement-based approaches or between measurements and models are larger than those at a global scale.

An ensemble of five model simulations gives a DRE that is about 30-50% smaller than the measurement-based estimate. Such discrepancy could be reduced to 15-40% after accounting for cloud contamination in satellite retrievals. The integration of satellite and surface measurements into a *CTM* proves to be a promising and essential approach to producing an optimal description of aerosol distributions and hence aerosol radiative.

Using the quantitative separation of fine and coarse aerosol in enhanced new-generation satellite sensors, the cloud-free DCF by anthropogenic aerosols is estimated to be -1.1±0.37 Wm^{-2} over ocean, about a factor of 2 stronger than model simulated -0.6 Wm^{-2}. Similar DCF estimates are rare over land, but a few studies do suggest that the DCF over land is much more negative than that over ocean. On global average, the measurement-based estimate of DCF ranges from -0.9~ -1.9 Wm^{-2}, again stronger than the model-based estimate of -0.8 Wm^{-2}. Overall, DCF estimates have larger uncertainty than DRE estimates do.

The use of high-quality aerosol measurements from remote sensing and in-situ techniques, along with the improved performance of model simulations in the past decade, has resulted in a new estimate of aerosol climate forcing with reduced uncertainties in IPCC AR4. The aerosol direct climate forcing is estimated to be -0.5±0.4 Wm^{-2} with a medium-low level of scientific understanding. The indirect forcing due to the cloud albedo effect for liquid water clouds is estimated to be -0.7 (ranging from -1.1 to +0.4) Wm^{-2}, with a low level of scientific understanding (Forster et al., 2007). In fact, such progress in quantifying the aerosol direct and indirect forcing plays an exclusively important role in the more definitive assessment of the global anthropogenic radiative forcing as *virtually certainly positive* and conversely *exceptionally unlikely negative* in IPCC AR4 (Haywood and Schulz, 2007).

Despite the substantial progress, several important issues remain, such as measurements of aerosol size distribution, particle shape, absorption, and vertical profiles, and detection of aerosol long-term trend and establishment of its connection with the observed trends of solar radiation reaching the surface. Significant efforts are needed to address them. Current observational capability needs to be continued to construct a long-term data record with consistent accuracy and high quality that can be used to detect long-term trends of aerosol. Along with algorithm refinement for better aerosol optical depth retrievals, future measurements should focus on improved retrievals of such aerosol properties as size distribution, particle shape, absorption, and vertical distribution. Coordinated sub-orbital measurements need to be conducted in context of evaluating and validating remote sensing measurements.

These new measurements are essential to reducing uncertainties associated with the estimate of aerosol climate forcing, in particular the anthropogenic fraction of aerosol, aerosol TOA forcing over land, aerosol forcing at the surface, and aerosol induced increment of atmospheric heating rate profile. Coordinated research strategy need to be developed to synthesize measurements from multiple platforms and sensors for a better characterization of complex aerosol system and to integrate remote sensing measurements into models for a stronger constraint of model simulations.

Finally, *aerosol-cloud interactions* continue to be an enormous challenge from both the observational and modeling perspectives, and progress is crucial if we are to improve our ability to predict climate change. The relatively short lifetimes of aerosol particles (order of days), in addition to the even shorter timescales for cloud formation and dissipation (10s of minutes) make this a particularly difficult challenge. Moreover, the problem requires addressing an enormous range of spatial scales, from the microscale to the global scale. A methodology for integrating observations (in-situ and remote) and models at the range of relevant temporal/spatial scales is crucial if we are to make progress on this problem.

References

Abdou W., D. Diner, J. Martonchik, C. Bruegge, R. Kahn, B. Gaitley, and K. Crean, 2005: Comparison of conincident MISR and MODIS aerosol optical depths over land and ocean scenes containing AERONET sites. *J. Geophys. Res.* **110:** D10S07, doi:10.1029/2004JD004693.

Ackerman A., O. Toon, D. Stevens, A. Heymsfield, V. Ramanathan, and E. Welton, 2000: Reduction of tropical cloudiness by soot. *Science* **288**:1042-1047.

Ackerman T., and G. Stokes, 2003: The Atmospheric Radiation Measurement Program. *Physics Today* **56**:38-44.

Albrecht B., 1989: Aerosols, cloud microphysics, and fractional cloudiness. *Science* **245**:1227-1230.

Alpert P., P. Kishcha, Y. Kaufman, and R. Schwarzbard, 2005: Global dimming or local dimming? Effect of urbanization on sunlight availability. *Geophys. Res. Lett.* **32:**L17802, doi: 10.1029/GL023320.

Anderson T., R. Charlson, S. Schwartz, R. Knutti, O. Boucher, H. Rodhe, and J. Heintzenberg, 2003a: Climate forcing by aerosols - A hazy picture. *Science* **300**:1103-1104.

Anderson T., R. Charlson, D. Winker, J. Ogren, and K. Holmén, 2003b: Mesoscale variations of tropospheric aerosols. *J. Atmos. Sci.,* **60**:119-136.

Anderson T., R. Charlson, N. Bellouin, O. Boucher, M. Chin, S. Christopher, J. Haywood, Y. Kaufman, S. Kinne, J. Ogren, L. Remer, T. Takemura, D. Tanré, O. Torres, C. Trepte, B. Wielicki, D. Winker, and H. Yu, 2005a.: An "A-Train" strategy for quantifying direct aerosol forcing of climate. *Bull. Am. Met. Soc.* **86**:1795-1809.

Anderson T., Y. Wu, D. Chu, B. Schmid, J. Redemann, and O. Dubovik, 2005b: Testing the MODIS satellite retrieval of aerosol fine-mode fraction. *J. Geophys. Res.* **110**: D18204, doi:10.1029/2005JD005978.

Andreae M. O., D. Rosenfeld, P. Artaxo, et al., 2004: Smoking rain clouds over the Amazon. *Science* **303**:1337– 1342.

Arnott W., H. Moosmuller, and C. Rogers, 1997: Photoacoustic spectrometer for measuring light absorption by aerosol: instrument description. *Atmos. Environ.* **33**:2845-2852.

Balkanski Y., M. Schulz, T. Claquin, and S. Guibert, 2007: Reevaluation of mineral aerosol radiative forcings suggests a better agreement with satellite and AERONET data. *Atmos. Chem. Phys.* **7**:81-95.

Bates T., B. Huebert, J. Gras, F. Griffiths, and P. Durkee (1998): The International Global Atmospheric Chemistry (IGAC) Project's First Aerosol Characterization Experiment (ACE-1) - Overview. *J. Geophys. Res*. **103:**16,297-16,318.

Bates T., P. Quinn, D. Coffman, D. Covert, T. Miller, J. Johnson, G. Carmichael, S. uazzotti, D. Sodeman, K. Prather, M. Rivera, L. Russell, and J. Merrill, 2004: Marine boundary layer dust and pollution transport associated with the passage of a frontal system over eastern Asia. *J. Geophys. Res.* **109:**doi:10.1029/2003JD004094.

Bates T., et al., 2006: Aerosol direct radiative effects over the northwestern Atlantic, northwestern Pacific, and North Indian Oceans: estimates based on in-situ chemical and optical measurements and chemical transport modeling. *Atmos. Cehm. Phys.*, **6**:1657-1732.

Bellouin N., O. Boucher, D. Tanré, and O. Dubovik, 2003: Aerosol absorption over the clear-sky oceans deduced from POLDER-1 and AERONET observations. *Geophys. Res. Lett.* **30**:1748, doi:10.1029/2003GL017121.

Bellouin N., O. Boucher, J. Haywood, and M. Reddy, 2005: Global estimates of aerosol direct radiative forcing from satellite measurements. *Nature* **438**:1138-1140, doi:10.1038/nature04348.

Bellouin N., A. Jones, J. Haywood, and S.A. Christopher, 2008: Updated estimate of aerosol direct radiative forcing from satellite observations and comparison against the Hadley Centre climate model. *J. Geophys. Res.* **113**:D10205, doi:10.1029/2007JD009385.

Bond T., and R. Bergstrom, 2006: Light absorption by carbonaceous particles: An investigative review. *Aerosol Sci. Technol*. **40**:27-67.

Boucher O., and D. Tanré, 2000: Estimation of the aerosol perturbation to the Earth's radiative budget over oceans using POLDER satellite aerosol retrievals. *Geophys. Res. Lett.* **27**:1103-1106.

Brennan J., Y. Kaufman, I. Koren, I., and R. Li, 2005: Aerosol-cloud interaction — misclassification of MODIS clouds in heavy aerosol. *IEEE Trans. Geos. Rem. Sens.* **43(4)**:911-915.

Carmichael G., G. Calori, H. Hayami, I. Uno, S. Cho, M. Engardt, S. Kim, Y. Ichikawa, Y. Ikeda, J. Woo, H. Ueda and M. Amann, 2002: The Mics-Asia study: Model intercomparison of long-range transport and sulfur deposition in East Asia. *Atmos. Environ.* **36**:175-199.

Carmichael G., Y. Tang, G. Kurata, I. Uno, D. Streets, N. Thongboonchoo, J. Woo, S. Guttikunda, A. White, T. Wang, D. Blake, E. Atlas, A. Fried, B. Potter, M. Avery, G. Sachse, S. Sandholm, Y. Kondo, R. Talbot, A. Bandy, D. Thorton and A. Clarke, 2003: Evaluating regional emission estimates using the TRACE-P observations. *J. Geophys. Res.* **108**:8810, doi:10.1029/2002JD003116.

Carrico C. et al., 2005: Hygroscopic growth behavior of a carbon-dominated aerosol in Yosemite National Park. *Atmos. Environ.* **39**:1393 – 1404.

Cattrall C., K. Carder, and H. Gordon, 2003: Columnar aerosol single-scattering albedo and phase function retrieved from sky radiance over the ocean: Measurements of Saharan dust. *J. Geophys. Res.* **108**:4287, doi:10.1029/2002JD002497.

Charlson, R., S. Schwartz, J. Hales, R. Cess, R. J. Coakley, Jr., J. Hansen, and D. Hofmann, 1992: Climate forcing by anthropogenic aerosols. *Science* **255**:423-430.

Chin M., R. Rood, S. Lin, J. Muller, and A. Thompson, 2000a: Atmospheric sulfur cycle simulated in the global model GOCART: Model description and global properties. *J. Geophys. Res.* **105**:24671-24687.

Chin M., D. Savoie, B. Huebert, A. Bandy, D. Thornton, T. Bates, P. Quinn, E. Saltzman, and W. De Bruyn, 2000b: Atmospheric sulfur cycle simulated in the global model GOCART: Comparison with field observations and regional budgets. *J. Geophys. Res.*, **105**:24689-24712.

Chin M., P. Ginoux, S. Kinne, O. Torres, B. Holben, B. Duncan, R. Martin, J. Logan, A. Higurashi, and T. Nakajima, 2002: Tropospheric aerosol optical thickness from the GOCART model and comparisons with satellite and sun photometer measurements. *J. Atmos., Sci.* **59**:461-483.

Chin M., P. Ginoux, R. Lucchesi, B. Huebert, R. Weber, T. Anderson, S. Masonis, B. Blomquist, A. Bandy, and D. Thornton, 2003: A global aerosol model forecast for the ACE-Asia field experiment. *J. Geophys. Res.,* **108**:8654, doi:10.1029/2003JD003642,.

Chin, M., D. Chu, R. Levy, L. Remer, Y. Kaufman, B. Holben, T. Eck, and P. Ginoux, 2004: Aerosol distribution in the northern hemisphere during ACE-Asia: Results from global model, satellite observations, and sunphotometer measurements. *J. Geophy. Res.* **109**:D23S90, doi:10.1029/2004JD004829.

Chou M., P. Chan, and M. Wang, 2002: Aerosol radiative forcing derived from SeaWiFS-retrieved aerosol optical properties. *J. Atmos. Sci.*. **59**:748-757.

Christopher S., and J. Zhang, 2002a: Shortwave aerosol radiative forcing from MODIS and CERES observations over the oceans. *Geophys. Res., Lett.* **29**:1859, doi:10.1029/2002GL014803.

Christopher S., J. Zhang, Y. Kaufman, and L. Remer, 2006: Satellite-based assessment of top of atmosphere anthropogenic aerosol radiative forcing over cloud-free oceans. *Geophys. Res. Lett.* **33:**L15816.

Chu D., Y. Kaufman, C. Ichoku, L. Remer, D. Tanré, and B. Holben, 2002: Validation of MODIS aerosol optical depth retrieval over land. *Geophys. Res. Lett.* **29**, doi:10.1029/2001/GL013205.

Chung C., V. Ramanathan, D. Kim, and I. Podgomy, 2005: Global anthropogenic aerosol direct forcing derived from satellite and ground-based observations. *J. Geophys. Res.* **110:**D24207, doi:10.1029/2005JD006356.

Clarke A., and R. Charlson, 1985: Radiative properties of the background aerosol: Absorption component of extinction. *Science* **229**:263-265.

Collins W., P. Rasch, B. Eaton, B. Khattatov, J. Lamarque, and C. Zender, 2001.: Simulating aerosols using a chemical transport model with assimilation of satellite aerosol retrievals: Methodology for INDOEX. *J. Geophys. Res.* **106**:7313—7336.

Costa M., A. Silva, and V. Levizzani, 2004a: Aerosol characterization and direct radiative forcing assessment over the ocean. Part I: Methodology and sensitivity analysis. *J. Appl. Meteorol.* **43:**1799-1817.

Costa M., A. Silva AM, and V. Levizzani, 2004b: Aerosol characterization and direct radiative forcing assessment over the ocean. Part II: Application to test cases and validation. *J. Appl. Meteorol.* **43:**1818-1833.

de Gouw J., et al., 2005: Budget of organic carbon in a polluted atmosphere: Results from the New England Air Quality Study in 2002. *J. Geophys. Res.* **110:**D16305, doi:10.1029/2004JD005623.

Delene D. and J. Ogren, 2002: Variability of aerosol optical properties at four North American surface monitoring sites. *J. Atmos. Sci.* **59**:1135-1150.

Deuzé J., F. Bréon, C. Devaux, P. Goloub, M. Herman, B. Lafrance, F. Maignan, A. Marchand, F. Nadal, G. Perry, and Tanré, D.: Remote sensing of aerosols over land surfaces from POLDER-ADEOS-1 polarized measurements. *J. Geophys. Res.* **106**:4913-4926, 2001.

Diner, D., J. Beckert, T. Reilly, et al., 1998: Multiangle Imaging SptectrRadiometer (MISR) description and experiment overview. *IEEE Trans. Geosci. Remote. Sens.* **36**:1072-1087.

Diner D., J. Beckert, G. Bothwell and J. Rodriguez, J2002: Performance of the MISR instrument during its first 20 months in Earth orbit. *IEEE Trans. Geosci. Remote Sens.* **40**:1449-1466.

Diner D., T. Ackerman, T. Anderson, et al.: Progressive Aerosol Retrieval and Assimilation Global Observing Network (PARAGON): An integrated approach for characterizing aerosol climatic and environmental interactions. *Bull. Amer. Meteo. Soc.,* **85**:1491-1501.

Dubovik O., A. Smirnov, B. Holben, M. King, Y. Kaufman, and Slutsker, 2000: Accuracy assessments of aerosol optical properties retrieved from AERONET sun and sky radiance measurements. *J. Geophys. Res.* **105**:9791-9806.

Dubovik O., and M. King, 2000: A flexible inversion algorithm for retrieval of aerosol optical properties from Sun and sky radiance measurements. *J. Geophys. Res.,* **105:**20673-20696.

Dubovik O., B. Holben, T. Eck, A. Smirnov, Y. Kaufman,]M. King, D. Tanré, and I. Slutsker, 2002: Variability of absorption and optical properties of key aerosol types observed in worldwide locations. *J. Atmos. Sci.* **59:**590-608.

Dubovik O., T. Lapyonok, Y. Kaufman, M. Chin, P. Ginoux, and A. Sinyuk, 2007: Retrieving global sources of aerosols from MODIS observations by inverting GOCART model, *Atmos. Chem. Phys. Discuss.* **7**:3629-3718.

Dufresne J., C. Gautier, P. Ricchizzi, and Y. Fouquart, 2002: Longwave scattering effects of mineral aerosols. *J. Atmos. Sci.,* **59**:1959-1966.

Eck T., B. Holben, J. Reid, O. Dubovik, A. Smirnov, N. O'Neill, I. Slutsker, and S. Kinne, 1999: Wavelength dependence of the optical depth of biomass burning, urban and desert dust aerosols. *J. Geophys. Res.* **104**:31333-31350.

Eck T., B. Holben, and J. Reid, et al., 2003: High aerosol optical depth biomass burning events: A comparison of optical properties for different source regions. *Geophys. Res. Lett.*, **30**:2035, doi:10.1029/2003GL017861.

Fehsenfeld F., et al., 2006:International Consortium for Atmospheric Research on Transport and Transformation (ICARTT): North America to Europe—Overview of the 2004 summer field study. *J. Geophys. Res.,* **111:**D23S01, doi:10.1029/2006JD007829.

Feingold G., W. Eberhard, D. Veron, and M. Previdi, 2003: First measurements of the Twomey aerosol indirect effect using ground-based remote sensors. *Geophys. Res. Lett.* **30**:1287, doi:10.1029/2002GL016633.

Feingold, G., Remer, L. A., Ramaprasad, J. and Kaufman, Y. J., 2001: Analysis of smoke impact on clouds in Brazilian biomass burning regions: An extension of Twomey's approach., J. Geophys. Res., **106**, 22,907-922,922.

Feingold G., H. Jiang, and J. Harrington, 2005: On smoke suppression of clouds in Amazonia. *Geophys. Res. Lett.* **32**:L02804, doi:10.1029/2004GL021369.

Ferrare R., D. Turner, L. Brasseur, W. Feltz, O. Dubovik, and T. Ackerman, 2001: Raman lidar measurements of the aerosol extinction-to-backscatter ratio over the Southern Great Plains. *J. Geophys. Res.,* **106**:20333-20347.

Ferrare R., G. Feingold, S. Ghan, J. Ogren, B. Schmid, S.E. Schwartz, and P. Sheridan, 2006: Preface to special section: Atmospheric Radiation Measurement Program May 2003 Intensive Operations Period examining aerosol properties and radiative influences. *J. Geophys. Res.* **111:**D05S01, doi:10.1029/2005JD006908.

Forster P., et al., 2007: Changes in Atmospheric Constituents and in Radiative Forcing. *In: Climate Change 2007: The Physical Science Basis, Contribution of Working Group I to the Fourth Assessment Report of the Intergovermental Panel on Climate Change* [Solomon, S., et al. (eds.)], Cambridge University Press, Cambridge, UK, and New York, NY, USA.

Fraser R. and Y. Kaufman, 1985: The relative importance of aerosol scattering and absorption in Remote Sensing. *Transactions on Geoscience and Remote Sensing,* GE-**23**:625-633.

GAMDT - Geophysical Fluid Dynamics Laboratory (GFDL) Global Atmospheric Model Development Team, 2004: The new GFDL global atmosphere and land model AM2-LM2: Evaluation with prescribed SST Simulations. *J. Climate,* **17:**4641-4673.

Garrett T., C. Zhao, X. Dong, G. Mace, and P. Hobbs, 2004: Effects of varying aerosol regimes on low-level Arctic stratus. *Geophys. Res. Lett.* **31:**L17105, doi:10.1029/2004GL019928.

Geogdzhayev I., M. Mishchenko, W. Rossow, B. Cairns, B., and A. Lacis, 2002: Global two-channel AVHRR retrievals of aerosol properties over the ocean for the period of NOAA-9 observations and preliminary retrievals using NOAA-7 and NOAA-11 data. *J. Atmos. Sci.*, **59**:262--278.

Ginoux P., M. Chin, I. Tegen, J. Prospero, B. Holben, O. Dubovik, and S. Lin, 2001: Sources and distributions of dust aerosols simulated with the GOCART model. *J. Geophys. Res.* **106:**20225-20273.

Ginoux P., J. Prospero, O. Torres, and M. Chin, 2004: Long-term simulation of dust distribution with the GOCART model: Correlation with the North Atlantic Oscillation. *Environ. Modeling and Software* **19**:113-128.

Han, Q., W. B. Rossow, J. Chou, and R. M. Welch, Global survey of the relationship of cloud albedo and liquid water path with droplet size using ISCCP, 1998: *J. Clim*., **11**, 1516– 1528.

Hansen J., M. Sato, and R. Ruedy, 1997: Radiative forcing and climate response. *J. Geophys. Res.* **102**:6831-6864.

Harrison L., J. Michalsky, and J. Berndt, 1994: Automated multifilter rotating shadowband radiometer: An instrument for optical depth and radiation measurements. *Applied Optics* **33**:5118-5125.

Haywood J. and K. Shine, 1995: The effect of anthropogenic sulfate and soot aerosol on the clear sky planetary radiation budget. *Geophys. Res. Lett*. **22**:603-606.

Haywood J., and O. Boucher, 2000: Estimates of the direct and indirect radiative forcing due to tropospheric aerosols: A review. *Rev. Geophys.* **38**:513-543.

Haywood J., P. Francis, S. Osborne, M. Glew, N. Loeb, E. Highwood, D. Tanré, E. Myhre, P. Formenti, and E. Hirst, 2003: Radiative properties and direct radiative effect of Saharan dust measured by the C-130 aircraft during SHADE: 1.Solar spectrum. *J. Geophys. Res.* **108**:8577, doi:10.1029/2002JD002687.

Haywood J., S. Osborne, and S. Abel, 2004: The effect of overlying absorbing aerosol layers on remote sensing retrievals of cloud effective radius and cloud optical depth. *Quart. J. Roy. Met. Soc.* **130**:779-800.

Haywood J., R. Allan, I. Culverwell, T. Slingo, S. Milton, J. Edwards, and N. Clerbaux, 2005: Can desert dust explain the outgoing longwave radiation anomaly over the Sahara during July 2003? *J. Geophys. Res.* **110**:D05105, doi:10.1029/2004JD005232.

Haywood J., and M. Schulz, 2007: Causes of the reduction in uncertainty in the anthropogenic radiative forcing of climate between IPCC (2001) and IPCC (2007). *Geophys. Res. Lett.* **34**:L20701, doi:10.1029/2007GL030749.

Heintzenberg J., H. Graf, R. Charlson, and P. Warneck, 1996: Climate forcing and the physicochemical life cycle of the atmospheric aerosol - Why do we need an integrated, interdisciplinary global research programme? *Beitr. Phys. Atmosph.* **69**:261-271.

Heintzenberg J., R. Charlson, A. Clarke, et al., 1997: Measurements and modeling of aerosol single-scattering albedo: progress, problems and prospects. *Beitr.Phys. Atmosph.* **70**:249-263.

Herman J., P. Bhartia, O. Torres, C. Hsu, C. Seftor, and E. Celarier, 1997: Global distribution of UV-absorbing aerosols from Nimbus-7/TOMS data. *J. Geophys. Res.* **102**:16911--16922.

Highwood E., J. Haywood, M. Silverstone, S. Newman, and J. Taylor 2003: Radiative properties and direct effect of Saharan dust measured by the C-130 aircraft during Saharan Dust Experiment (SHADE): 2. Terrestrial spectrum. *J. Geophys. Res.* **108**: 8578, doi:10.1029/2002JD002552.

Hoff R. et al., 2002: Regional East Atmospheric Lidar Mesonet: REALM, in *Lidar Remote Sensing in Atmospheric and Earth Sciences*, edited by L. Bissonette, G. Roy, and G. Vallée, pp. 281-284, Def. R&D Can. Valcartier, Val-Bélair, Que..

Hoff R., J. Engel-Cox, N. Krotkov, S. Palm, R. Rogers, K. McCann, L. Sparling, N. Jordan, O. Torres, and J. Spinhirne, 2004: Long-range transport observations of two large forest fire plumes to the northeastern U.S., in *22nd International Laser Radar Conference, ESA Spec. Publ., SP-***561**:683-686.

Holben B., T. Eck, I. Slutsker, et al., 1998: AERONET - A federated instrument network and data archive for aerosol characterization. *Remote Sens. Environ.* **66**:1-16.

Holben B., D. Tanré, A. Smirnov, et al., 2001: An emerging ground-based aerosol climatology: aerosol optical depth from AERONET. *J. Geophys. Res.* **106**:12067-12098.

Horvath H., 1993: Atmospheric light absorption -- A review. *Atmos. Environ.* **27A**:293-317.

Hsu N., S. Tsay, M. King, and J. Herman, 2004: Aerosol properties over bright-reflecting source regions. *IEEE Trans. Geosci. Remote Sens.* **42:**557-569.

Hsu N., J. Herman, and C. Weaver, 2000: Determination of radiative forcing of Saharan dust using combined TOMS and ERBE data. *J. Geophys. Res.* **105**:20649-20661.

Huebert B., T. Bates, P. Russell, G. Shi, Y. Kim, K. Kawamura, G. Carmichael, and T. Nakajima, 2003: An overview of ACE-Asia: strategies for quantifying the relationships between Asian aerosols and their climatic impacts. *J. Geophys. Res*. **108**:8633, doi:10.1029/2003JD003550.

Husar R., J. Prospero, and L. Stowe, 1997: Characterization of tropospheric aerosols over the oceans with the NOAA advanced very high resolution radiometer optical thickness operational product. *J. Geophys. Res.* **102**:16889-16909.

Ichoku C., L. Remer, and T. Eck, 2005: Quantitative evaluation and intercomparison of morning and afternoon MODIS aerosol measurements from Terra and Aqua satellites. *J. Geophys. Res.* **110**:D10S03, doi:10.1029/2004JD004987.

IPCC (Intergovernmental Panel on Climate Change), 2001: Radiative forcing of climate change, in Climate Change 2001, Cambridge Univ. Press, New York, Cambridge University Press, 2001.

Jacob D., J. Crawford, M. Kleb, V. Connors, R.J. Bendura, J. Raper, G. Sachse, J. Gille, L. Emmons, and C. Heald, 2003: The Transport and Chemical Evolution over the Pacific (TRACE-P) aircraft mission: design, execution, and first results. *J. Geophys. Res.* **108:**9000, 10.1029/2002JD003276.

Jacobson M., 2000: A physically-based treatment of elemental carbon optics: Implications for global direct forcing of aerosols. *Geophys. Res. Lett*. **27**:217-220.

Jacobson M., 2001: Strong radiative heating due to the mixing state of black carbon in atmospheric aerosols. *Nature* **409**:695-697.

Jeong M., Z. Li, D. Chu, and S. Tsay, 2005: Quality and Compatibility Analyses of Global Aerosol Products Derived from the Advanced Very High Resolution Radiometer and Moderate Resolution Imaging Spectroradiometer. *J. Geophys. Res.* **110**:D10S09, doi:10.1029/2004JD004648.

Jiang, H., and G. Feingold, 2006: Effect of aerosol on warm convective clouds: Aerosol-cloud-surface flux feedbacks in a new coupled large eddy model. *J. Geophys. Res.*, **111**: D01202, doi:10.1029/2005JD006138.

Kahn R., W. Li, C. Moroney, D. Diner, J. Martonchik, and E. Fishbein, 2007: Aerosol source plume physical characteristics from space-based multiangle imaging. *J. Geophys. Res.* **112**:D11205, doi:10.1029/2006JD007647.

Kahn R., R. Gaitley, J. Martonchik, D. Diner, K. Crean, and B. Holben, 2005a: MISR global aerosol optical depth validation based on two years of coincident AERONET observations. *J. Geophys. Res.*

110:D10S04, doi:10.1029/2004JD004706.

Kahn R., W. Li, J. Martonchik, C. Bruegge, D. Diner, B. Gaitley, W. Abdou, O. Dubovik, B. Holben, A. Smirnov, Z. Jin, and D. Clark, 2005b: MISR low-light-level calibration, and implications for aerosol retrieval over dark water. *J. Atmos. Sci.* **62:**1032-1052.

Kahn R., J. Ogren, T. Ackerman, et al., 2004a: Aerosol data sources and their roles within PARAGON. *Bull. Amer. Meteor. Soc.* **85**:1511-1522.

Kahn R., J. Anderson, T. Anderson, et al., 2004b: Environmental snapshots from ACE-Asia. *J. Geophys. Res.* **109**:doi:2003JD004339.

Kahn R., P. Banerjee, and D. McDonald, 2001: The sensitivity of multiangle imaging to natural mixtures of aerosols over ocean. *J. Geophys. Res.* **106**:18219-18238.

Kalashnikova O., R. Kahn, I. Sokolik, and W. Li, 2005: The ability of multi-angle remote sensing observations to identify and distinguish mineral dust types: Optical models and retrievals of optically thick plumes. *J. Geophys. Res.* **110**:D18S14, doi:10.1029/2004JD004550.

Kaufman Y., 1987: Satellite Sensing of Aerosol Absorption, *J. Geophys. Res.*, **92:**4307-4317.

Kaufman, Y. J. and Nakajima, T., 1993: Effect of Amazon smoke on cloud microphysics and albedo--Analysis from satellite imagery, *J. Applied Meteor*. **32**:729-744.

Kaufman, Y. and R. Fraser, 1997: The effect of smoke particles on clouds and climate forcing. *Science* **277**:1636-1639.

Kaufman Y., D. Tanré, L. Remer, E. Vermote, A. Chu, and B. Holben, 1997: Operational remote sensing of tropospheric aerosol over land from EOS moderate resolution imaging spectroradiometer. *J. Geophys. Res.* **102**:17051-17067.

Kaufman Y., B. Holben, D. Tanré, I. Slutsker, A. Smirnov, and T. Eck, 2000: Will aerosol measurements from Terra and Aqua polar orbiting satellites represent daily aerosol abundance and properties? *Geophys. Res. Lett.* **27**:3861-3864.

Kaufman Y., D. Tanré, O. Dubovik, A. Karnieli, and L. Remer, 2001: Absorption of sunlight by dust as inferred from satellite and ground-based measurements. *Geophys. Res., Lett.* **28**:1479-1482.

Kaufman Y., D. Tanré, and O. Boucher, 2002a: A satellite view of aerosols in the climate system. *Nature* **419**: doi:10.1038/nature01091.

Kaufman Y., J. Martins, L. Remer, M. Schoeberl, and M. Yamasoe, 2002b: Satellite retrieval of aerosol absorption over the oceans using sunglint. *Geophys. Res. Lett.* **29**: 1928, doi:10.1029/2002GL015403.

Kaufman Y., J. Haywood, P. Hobbs, W. Hart, R. Kleidman, and B. Schmid, 2003: Remote sensing of vertical distributions of smoke aerosol off the coast of Africa. *Geophys. Res. Lett.* **30**:1831, doi:10.1029/2003GL017068.

Kaufman Y., O. Boucher, D. Tanré, M. Chin, L. Remer, and T. Takemura, 2005a: Aerosol anthropogenic component estimated from satellite data. *Geophys. Res. Let.* **32**: L17804, doi:10.1029/2005GL023125.

Kaufman Y., L. Remer, D. Tanré, R. Li, R. Kleidman, S. Mattoo, R. Levy, T. Eck, B. Holben, C. Ichoku, J. Martins, and I. Koren, 2005b: A critical examination of the residual cloud contamination and diurnal sampling effects on MODIS estimates of aerosol over ocean. *IEEE Trans. on Geoscience & Remote Sensing,* **43**:2886-2897.

Kaufman, Y. J., I. Koren, L. A. Remer, D. Rosenfeld and Y. Rudich, 2005: The effect of smoke, dust, and pollution aerosol on shallow cloud development over the Atlantic Ocean, *Proc. Nat. Acad. Sci*., **102**:11207-11212.

Kaufman, Y. J. and Koren, I., 2006: Smoke and pollution aerosol effect on cloud cover. *Science* **313**:655-658.

Keil A., and J. Haywood, 2003: Solar radiative forcing by biomass burning aerosol particles during SAFARI-2000: A case study based on measured aerosol and cloud properties. *J. Geophys. Res.* **108**:8467, doi:10.1029/2002JD002315.

Kim B.-G., S. Schwartz, M. Miller, and Q. Min, 2003: Effective radius of cloud droplets by ground-based remote sensing: Relationship to aerosol. *J. Geophys. Res.* **108**:4740, doi:10.1029/2003JD003721.

King M., Y. Kaufman, D. Tanré, and T. Nakajima, 1999: Remote sensing of tropospheric aerosols: Past, present, and future. *Bull. Am. Meteorol. Soc.* **80**:2229-2259.

King M., S. Platnick, C. Moeller, Revercomb, and D. Chu, 2003: Remote sensing of smoke, land, and clouds from the NASA ER-2 during SAFARI 2000. *J. Geophys. Res.* **108:**8502, doi:10.1029/2002JD003207.

Kinne S., M. Schulz, C. Textor, et al., 2006: An AeroCom initial assessment -- optical properties in aerosol component modules of global models. *Atmos. Chem. Phys.* **6**:1815-1834.

Kleidman R., N. O'Neill, L. Remer, Y. Kaufman, T. Eck, D. Tanré, O. Dubovik, and B. Holben, 2005: Comparison of Moderate Resolution Imaging Spectroradiometer (MODIS) and Aerosol Robotic Network (AERONET) remote-sensing retrievals of aerosol fine mode fraction over ocean. *J. Geophys. Res.* **110**:D22205, doi:10.1029/2005JD005760.

Koch D., and J. Hansen, 2005: Distant origins of Arctic black carbon: A Goddard Institute for Space Studies ModelE experiment. *J. Geophys. Res.* **110**: D04204, doi:10.1029/2004JD005296.

Koch D., G. Schmidt, and C. Field, 2006: Sulfur, sea salt and radionuclide aerosols in GISS ModelE. *J. Geophys. Res.* **111**:D06206, doi:10.1029/2004JD005550.

Koren I., Y. Kaufman, L. Remer, and J. Martins, 2004: Measurement of the effect of Amazon smoke on inhibition of cloud formation. *Science* **303**:1342.

Koren, I., Kaufman, Y. J., Rosenfeld, D., Remer, L. A. and Rudich, Y., 2005: Aerosol invigoration and restructuring of Atlantic convective clouds, *Geophys. Res. Lett.*, **32**:doi:10.1029/2005GL023187.

Koren I., L. Remer, Y. Kaufman, Y. Rudich, and J. Martins, 2007a: On the twilight zone between clouds and aerosols. *Geophys. Res. Lett.* **34**:L08805, doi:10.1029/2007GL029253.

Koren I., L. Remer, and K. Longo, 2007b: Reversal of trend of biomass burning in the Amazon. *Geophys. Res. Lett.* **34**: L20404, doi:10.1029/2007GL031530.

Lau K., M. Kim, and K. Kim, 2006: Asian summer monsoon anomalies induced by aerosol direct forcing - the role of the Tibetan Plateau. *Climate Dynamics* **36**:855-864, doi:10.1007/s00382-006-10114-z.

Leahy L., T. Anderson, T. Eck, and R. Bergstrom, 2007: A synthesis of single scattering albedo of biomass burning aerosol over southern Africa during SAFARI 2000. *Geophys. Res. Lett.* **34:**L12814, doi:10.1029/2007GL029697.

Lee T., et al., 2006: The NPOESS VIIRS day/night visible sensor. *Bull. Amer. Meteorol. Soc.* **87**:191-199.

Léon J., D. Tanré, J. Pelon, Y. Kaufman, J. Haywood, and B. Chatenet, 2003: Profiling of a Saharan dust outbreak based on a synergy between active and passive remote sensing. *J. Geophys. Res.* **108**:8575, doi:10.1029/2002JD002774.

Levy R., L. Remer, and O. Dubovik, 2007a: Global aerosol optical properties and application to MODIS aerosol retrieval over land. *J. Geophys. Res.* **112**:D13210, doi:10.1029/2006JD007815.

Levy R., L. Remer, S. Mattoo, E. Vermote, and Y. Kaufman, 2007b: Second-generation algorithm for retrieving aerosol properties over land from MODIS spectral reflectance. *J. Geophys. Res.* **112**:D13211, doi:10.1029/2006JD007811.

Li Z., et al., 2007: Preface to special section on East Asian studies of tropospheric aerosols: An international regional experiment (EAST-AIRE). *J. Geophys. Res.* **112:**D22s00, doi:10.0129/2007JD008853.

Liu H., R. Pinker, and B. Holben, 2005: A global view of aerosols from merged transport models, satellite, and ground observations. *J. Geophys. Res.* **110**:D10S15, doi:10.1029/2004JD004695.

Liu X., J. Penner, B. Das, D. Bergmann, J. Rodriguez, S. Strahan, M. Wang, and Y. Feng, 2007: Uncertainties in global aerosol simulations: Assessment using three meteorological data sets. *J. Geophys. Res.*, **112**:D11212, doi: 10.1029/2006JD008216.

Li R., Y. Kaufman, W. Hao, I. Salmon, and B. Gao, 2004: A technique for detecting burn scars using MODIS data. *IEEE Trans. on Geoscience & Remote Sensing* **42**:1300-1308.

Loeb N., and S. Kato, 2002: Top-of-atmosphere direct radiative effect of aerosols over the tropical oceans from the Clouds and the Earth's Radiant Energy System (CERES) satellite instrument. *J. Climate* **15**:1474-1484.

Loeb N., and N. Manalo-Smith, 2005: Top-of-Atmosphere direct radiative effect of aerosols over global oceans from merged CERES and MODIS observations. *J. Clim.* **18**:3506-3526.

Lubin D., S. Satheesh, G. McFarquar, and A. Heymsfield, 2002: Longwave radiative forcing of Indian Ocean tropospheric aerosol. *J. Geophys. Res.* **107**:8004, doi:10.1029/2001JD001183.

Luo Y., D. Lu, X. Zhou, W. Li, and Q. He, 2001: Characteristics of the spatial distribution and yearly variation of aerosol optical depth over China in last 30 years. *J. Geophys. Res.* **106**:14501, doi:10.1029/2001JD900030.

Magi B., P. Hobbs, T. Kirchstetter, T. Novakov, D. Hegg, S. Gao, J. Redemann, and B. Schmid, 2005: Aerosol properties and chemical apportionment of aerosol optical depth at locations off the United States East Coast in July and August 2001. *J. Atmos. Sci.* **62**:919-933.

Malm W., J. Sisler, D. Huffman, R. Eldred, and T. Cahill, 1994: Spatial and seasonal trends in particle concentration and optical extinction in the United States. *J. Geophys. Res.* **99:**1347-1370.

Marshak, A., Knyazikhin, Y., Evans, K., and Wiscombe, W.: The "RED versus NIR" plane to retrieve broken-cloud optical depth from ground-based measurements. *J. Atmos. Sci.* **61:**1911-1925, 2004.

Martins J., P. Artaxo, C. Liousse, J. Reid, P. Hobbs, and Y. Kaufman, 1998: Effects of black carbon content, particle size, and mixing on light absorption by aerosols from biomass burning in Brazil. *J. Geophys. Res.* **103**:32041-32050, 1998.

Martins J., D. Tanré, L. Remer, Y. Kaufman, S. Mattoo, and R. Levy, 2002: MODIS cloud screening for remote sensing of aerosol over oceans using spatial variability. Geophys. Res. Lett. **29:**10.1029/2001GL013252.

Martonchik J., D. Diner, B. Pinty, M. Verstraete, R. Myneni, Y. Knjazikhin, and H. Gordon, 1998b: Determination of land and ocean reflective, radiative, and biophysical properties using multiangle imaging. *IEEE Trans. Geosci. Remote Sens.* **36**:1266-1281.

Martonchik J., D. Diner,R. Kahn, M. Verstraete, B. Pinty, H. Gordon, and T. Ackerman, 1998a: Techniques for the Retrieval of aerosol properties over land and ocean using multiangle data. *IEEE Trans. Geosci. Remt. Sensing* **36**:1212-1227

Martonchik J., D. Diner, K. Crean, and M. Bull, 2002: Regional aerosol retrieval results from MISR. *IEEE Trans. Geosci. Remote Sens.* **40**:1520-1531.

Massie S., O. Torres, and S. Smith, 2004: Total ozone mapping spectrometer (TOMS) observations of increases in Asian aerosol in winter from 1979 to 2000. *J. Geophys. Res.*, **109**:D18211, doi:10.1029/2004JD004620.

Matsui T., and R. Pielke, Sr., 2006: Measurement-based estimation of the spatial gradient of aeroosl radiative forcing. *Geophys. Res. Lett.* **33**: L11813, doi:10.1029/2006GL025974.

Matthis I., A. Ansmann, D. Müller, U. Wandinger, and D. Althausen, 2004: Multiyear aerosol observations with dual-wavelength Raman lidar in the framework of EARLINET. *J. Geophys. Res.* **109**:D13203, doi:10.1029/2004JD004600.

Michalsky J., J. Schlemmer, W. Berkheiser, et al., 2001: Multiyear measurements of aerosol optical depth in the Atmospheric Radiation Measurement and Quantitative Links program. *J. Geophys. Res.* **106:**12099-12108.

Miller R., R. Cakmur, J. Perlwitz, D. Koch, G. Schmidt, I. Geogdzhayev, P. Ginoux, C. Prigent, and I. Tegen, 2006: Mineral dust aerosols in the NASA Goddard Institute for Space Sciences ModelE atmospheric general circulation model. *J. Geophys. Res.*, **111**:D06208, doi:10.1029/2005JD005796.

Min Q., and L.C. Harrison, 1996: Cloud properties derived from surface MFRSR measurements and comparison with GEOS results at the ARM SGP site. *Geophys. Res. Lett.* **23:**1641- 1644.

Mishchenko M., I. Geogdzhayev, B. Cairns, W. Rossow, and A. Lacis, 1999: Aerosol retrievals over the ocean by use of channels 1 and 2 AVHRR data: Sensitivity analysis and preliminary results. *Appl. Opt.*, **38**:7325-7341.

Mishchenko M., et al., 2007a: Accurate monitoring of terrestrial aerosols and total solar irradiance. *Bull. Amer. Meteorol. Soc.* **88**:677-691.

Mishchenko M., et al., 2007b: Long-term satellite record reveals likely recent aerosol trend. *Science* **315**:1543.

Moody E., M. King, S. Platnick, C. Schaaf, and F. Gao, 2005: Spatially complete global spectral surface albedos: value-added datasets derived from Terra MODIS land products. *IEEE Trans. Geosci. Remote Sens.* **43**:144-158.

Moulin C., H. Godon, V. Banzon, and R. Evans, 2001: Assessment of Sahran dust absorption in the visible from SeaWiFS imagery. *J. Geophys. Res.* **106**:18239-18249.

Murayama T., N. Sugimoto, I. Uno, I., et al., 2001: Ground-based network observation of Asian dust events of April 1998 in East Asia. *J. Geophys. Res.* **106**:18346-18359.

NRC (National Research Council)**,** 2005: Radiative Forcing of Climate Change: Expanding the Concept and Addessing Uncertainties, National Academy Press, Washington D.C. (Available at http://www.nap.edu/openbook/0309095069/html).

NRC (National Research Council), 2001: Climate Change Sciences: An analysis of some key questions, 42pp., National Academy Press, Washington D.C..

Nakajima, T., Higurashi, A., Kawamoto, K. and Penner, J. E., 2001: A possible correlation between satellite-derived cloud and aerosol microphysical parameters., *Geophys. Res. Lett*. **28**:1171-1174.

Norris J., and M. Wild, 2007: Trends in aerosol radiative effects over Europe inferred from observed cloud cover, solar "dimming", and solar "brightening". *J. Geophys. Res.* **112**:D08214, doi:10.1029/2006JD007794.

Novakov T., V. Ramanathan, J. Hansen, T. Kirchstetter, M. Sato, J. Sinton, and J. Sathaye, 2003: Large historical changes of fossil-fuel black carbon emissions. *Geophys. Res. Lett.* **30**:1324, doi:10.1029/2002GL016345.

O'Neill N., T. Eck, A. Smirnov, B. .Holben, and S. Thulasiraman, 2003: Spectral discrimination of coarse and fine mode optical depth. J. Geophys. Res., 108(D17), 4559, doi:10.1029/2002JD002975.

Patterson E., D. Gillete, and B. Stockton, 1977: Complex index of refraction between 300 and 700 nm for Sahara aerosol. *J. Geophys. Res.* **82**:3153-3160.

Penner J., R. Dickinson, and C. O'Neill, 1992: Effects of aerosol from biomass burning on the global radiation budget. *Science* **256**:1432-1434.

Penner J., R. Charlson, J. Hales, et al., 1994: Quantifying and minimizing uncertainty of climate forcing by anthropogenic aerosols, *Bull. Amer. Meteorol. Soc.* **75**:375-400.

Penner J., S. Zhang, M. Chin, et al., 2002: A comparison of model- and satellite-derived aerosol optical depth and reflectivity. *J. Atmos. Sci.* **59**:441--460.

Pinker R., B. Zhang, and E. Dutton, 2005: Do satellite detect trends in surface solar radiation? *Science* **308**:850-854.

Qian Y., W. Wang, L Leung, and D. Kaiser, 2007: Variability of solar radiation under cloud-free skies in China: The role of aerosols. *Geophys. Res. Lett.* **34**:L12804, doi:10.1029/2006GL028800.

Quaas J., O. Boucher, N. Bellouin, and S. Kinne, 2008: Satellite-based estimate of the direct and indirect aerosol climate forcing. *J. Geophys. Res.* **113:**D05204, doi:10.1029/2007JD008962.

Quinn P., T. Anderson, T. Bates, R. Dlugi, J. Heintzenberg, W. Von Hoyningen-Huene, M. Kumula, P. Russel, and E. Swietlicki, 1996: Closure in tropospheric aerosol-climate research: A review and future needs for addressing aerosol direct shortwave radiative forcing. *Contrib. Atmosph. Phys.* **69**:547-577.

Quinn P., D. Coffman, V. Kapustin, T.S. Bates and D.S. Covert, 1998: Aerosol optical properties in the marine boundary layer during ACE 1 and the underlying chemical and physical aerosol properties. *J. Geophys. Res.* **103:**16547 - 16563.

Quinn P. T. Bates, T. Miller, D. Coffman, J. Johnson, J. Harris, J. Ogren, G. Forbes, G., T. Anderson, D. Covert, and M. Rood, 2000: Surface submicron aerosol chemical composition: What fraction is not sulfate? *J. Geophys. Res.* **105**:6785 - 6806.

Quinn P., and T. Bates, 2003: North American, Asian, and Indian haze: Similar regional impacts on climate? *Geophys. Res. Letts.* **30**:1555, doi:10.1029/2003GL016934.

Quinn P. and T. Bates, 2005: Regional Aerosol Properties: Comparisons from ACE 1, ACE 2, Aerosols99, INDOEX, ACE Asia, TARFOX, and NEAQS. *J. Geophys. Res.* **110:**D14202, doi:10.1029/2004JD004755,.

Quinn P., et al., 2005: Impact of particulate organic matter on the relative humidity dependence of light scattering: A simplified parameterization. *Geophys. Res. Lett.,* **32:**L22809, doi:101029/2005GL024322.

Quinn P., T. Bates, D. Coffman, T. Onasch, D. Worsnop, T. Baynard, J. de Gouw, P. Goldan, W. Kuster, E. Williams, J. Roberts, B. Lerner, A. Stohl, A. Pettersson, and E. Lovejoy, 2006: Impacts of sources and aging on submicrometer aerosol properties in the marine boundary layer across the Gulf of Maine. *J. Geophys. Res.* **111:**D23S36, doi:10.1029/2006JD007582.

Raes F., T. Bates, F. McGovern, and M. van Liedekerke, 2000: The 2nd Aerosol Characterization Experiment (ACE-2): General overview and main results. *Tellus* **52B:**111–125.

Ramanathan V., and A. Vogelmann, 1997: Greenhouse Effect, Atmospheric Solar Absorption, and the Earth's Radiation Budget: From the Arrhenius-Langely Era to the 1990's. *Ambio* ***26*:**38-46.

Ramanathan V., P. Crutzen, J. Lelieveld, et al., 2001: Indian Ocean Experiment: An integrated analysis of the climate forcing and effects of the great Indo-Asian haze. *J. Geophys. Res.* **106**:28371-28398.

Ramanathan V., and P. Crutzen, 2003: Atmospheric Brown "Clouds". *Atmos. Environ.* **37**:4033-4035.

Reddy M., and O.Boucher, 2004: A study of the global cycle of carbonaceous aerosols in the LMDZT general circulation model. *J. Geophys. Res.* **109**:D14202, doi:10.1029/2003JD004048.

Reddy M., O. Boucher, C. Venkataraman, S. Verma, J.-F. Le´on, N. Bellouin, and M. Pham, 2004: General circulation model estimates of aerosol transport and radiative forcing during the Indian Ocean Experiment. *J. Geophys. Res.* **109**:D16205, doi:10.1029/2004JD004557.

Reddy M., O. Boucher, N. Bellouin, M. Schulz, Y. Balkanski, J. Dufresne, and M. Pham, 2005a: Estimates of multi-component aerosol optical depth and direct radiative perturbation in the LMDZT general circulation model. *J. Geophys. Res.* **110**:D10S16, doi:10.1029/2004JD004757.

Reddy M., O. Boucher, Y. Balkanski, and M. Schulz, 2005b: Aerosol optical depths and direct radiative perturbations by species and source type. *Geophys. Res. Lett.* **32**: L12803, doi:10.1029/2004GL021743.

Redemann J., P. Russell, and P. Hamill, 2001: Dependence of aerosol light absorption and single-scattering albedo on ambient relative humidity for sulfate aerosols with black carbon cores. *J. Geophys. Res.* **106**:27485-27495.

Redemann J., S. Masonis, B. Schmid, T. Anderson, P. Russell, J. Livingston, O. Dubovik, and A. Clarke, 2003: Clear-column closure studies of aerosols and water vapor aboard the NCAR C-130 during ACE-Asia, 2001. *J. Geophys. Res.* **108:**8655, doi:10.1029/2003JD003442.

Reid J., J. Kinney, and D. Wesphal, et al., 2003: Analysis of measurements of Saharan dust by airborne and groundbased remote sensing methods during the Puerto Rico Dust Experiment (PRIDE). *J. Geophys. Res.* **108**:8586, doi:10.1029/2002JD002493.

Reid J., T. Eck, S. Christopher, R. Koppmann, O. Dubovik, D. Eleuterio, B. Holben, E. Reid, and J. Zhang, 2005: A review of biomass burning emissions part III: intensive optical properties of biomass bunring particles, *Atmos. Chem. Phys.* **5**:827-849.

Reid J., et al., 2008: An overview of UAE2 flight operations: Observations of summertime atmospheric thermodynamic and aerosol profiles of the southern Arabian Gulf. *J. Geophys. Res.* (Submitted).

Remer L., S. Gassó, D. Hegg, Y. Kaufman, and B. Holben, 1997: Urban/industrial aerosol: ground based sun/sky radiometer and airborne in-situ measurements. *J. Geophys. Res.* **102**:16849-16859.

Remer L., D. Tanré, Y. Kaufman, C. Ichoku, S. Mattoo, R. Levy, D. Chu, B. Holben, O. Dubovik, A. Smirnov, J. Martins, R. Li, and Z. Ahman, 2002: Validation of MODIS aerosol retrieval over ocean. *Geophys. Res. Lett.* **29**:doi:10.1029/2001/GL013204.

Remer L., Y. Kaufman, D. Tanré, S. Mattoo, D. Chu, J. Martins, R. Li, C. Ichoku, R. Levy, R. Kleidman, T. Eck, E. Vermote, and B. Holben, 2005: The MODIS aerosol algorithm, products and validation. *J. Atmos. Sci.* **62**:947-973.

Remer L., and Y. Kaufman, 2006: Aerosol direct radiative effect at the top of the atmosphere over cloud free ocean derived from four years of MODIS data. *Atmos. Chem. Phys.* **6**:237-253.

Remer L., Y. Kaufman, and R. Kleidman, 2006: Comparison of three years of Terra and Aqua MODIS aerosol optical thickness over the global oceans. *IEEE Geosci. Remote Sens. Lett.* **3:**537-540.

Rosenfeld D., and I. Lansky, 1998: Satellite-based insights into precipitation formation processes in continental and maritime convective clouds. *Bull. Am. Meteorol. Soc.* **79:**2457-2476.

Russell P., S. Kinne, and R. Bergstrom, 1997: Aerosol climate effects: local radiative forcing and column closure experiments. *J. Geophys. Res.* **102**:9397-9407.

Russell P., J. Livingston, P. Hignett, S. Kinne, J. Wong, A. Chien, R. Bergstrom, P. Durkee, and P. Hobbs, 1999: Aerosol-induced radiative flux changes off the United States mid-Atlantic coast: comparison of values calculated from sun photometer and in-situ data with those measured by airborne pyranometer. *J. Geophys. Res.* **104**:2289-2307.

Salcedo D., T. B. Onasch, K. Dzepina, M. R. Canagaratna, Q. Zhang, J.A. Huffman, P. F. DeCarlo, J. T. Jayne, P. Mortimer, D. R. Worsnop, C. E. Kolb, K. S. Johnson, B. Zuberi, L. C. Marr, R. Volkamer, L. T. Molina, M. J. Molina, B. Cardenas, R. M. BernabÎ, C. M‡rquez, J. S. Gaffney, N. A. Marley, A. Laskin, V. Shutthanandan, Y. Xie, W. Brune, R. Lesher, T. Shirley, and J. L. Jimenez, 2006: Characterization of ambient aerosols in Mexico City during the MCMA-2003 campaign with Aerosol Mass Spectrometry: results from the CENICA Supersite. *Atmos. Chem. Phys.* **6**:925-946.

Sato M., J. Hansen, D. Koch, A. Lacis, R. Ruedy, O. Dubovik, B. Holben, M. Chin, and T. Novakov, 2003: Global atmospheric black carbon inferred from AERONET. *Proc. Nat. Aca. Sci.* **100**:6319-6324.

Saxena P., L. Hildemann, P. McMurry, and J. Seinfeld, 1995: Organics alter hygroscopic behavior of atmospheric particles. *J. Geophys. Res.* **100:**18755-18770.

Schaaf C., F. Gao, A. Strahler, et al., 2002: First operational BRDF, albedo and nadir reflectance products from MODIS. *Remote Sens. Environ.* **83**:135-148.

Schmid B., R. Ferrare, C. Flynn, R. Elleman, D. Covert, A. Strawa, E. Welton, D. Turner, H. Jonsson, J. Redemann, J. Eilers, K. Ricci, A. Hallar, M. Clayton, J. Michalsky, A. Smirnov, B. Holben, and J. Barnard, 2006: How well do state-of-the-art techniques measuring the vertical profile of tropospheric aerosol extinction compare? *J. Geophys. Res.* **111:** doi:10.1029/2005JD005837, 2006.

Schulz M., C. Textor, S. Kinne, et al., 2006: Radiative forcing by aerosols as derived from the AeroCom present-day and pre-industrial simulations. *Atmos. Chem. Phys.*, **6**:5225-5246.

Sekiguchi, M., T. Nakajima, K. Suzuki, et al., A study of the direct and indirect effects of aerosols using global satellite data sets of aerosol and cloud parameters *J. Geophys. Res*, 108, NO. D22, 4699, doi:10.1029/2002JD003359, 2003

Seinfeld J., R. Kahn, T. Anderson, R. Charlson, R. Davies, D. Diner, S. Schwartz, and B. Wielicki, 2004: Scientific objectives, measurement needs, and challenges motivating the PARAGON aerosol initiative. *Bull. Amer. Meteo. Soc.* **85**:1503-1509.

Sheridan P., and J. Ogren, 1999: Observations of the vertical and regional variability of aerosol optical properties over central and eastern North America. *J. Geophys. Res.* **104**:16793-16805.

Slingo A., T. Ackerman, R. Allan, et al., 2006: Observations of the impact of a major Saharan dust storm on the atmospheric radiation balance. *Geophys. Res. Lett.* **33**:L24817, doi:10.1029/2006GL027869.

Smirnov A., B. Holben, T. Eck, O. Dubovik, and I. Slutsker, 2000: Cloud screening and quality control algorithms for the AERONET database. *Rem. Sens. Env.* **73**:337-349.

Smirnov A., B. Holben, T. Eck, I. Slutsker, B. Chatenet, and R. Pinker, 2002: Diurnal variability of aerosol optical depth observed at AERONET (Aerosol Robotic Network) sites. *Geophys. Res. Lett.* **29:**2115, doi:10.1029/2002GL016305.

Smirnov A., B. Holben, S. Sakerin, D. Kabanov, I. Slutsker, M. Chin, T. Diehl, L. Remer, R. Kahn, A. Ignatov, L. Liu, M. Mishchenko, T. Eck, T. Kucsera, D. Giles, and O. Kopelevich, 2006: Ship-based aerosol optical depth measurements in the Atlantic Ocean, comparison with satellite retrievals and GOCART model. *Geophys. Res. Lett.* **33:**L14817, doi: 10.1029/2006GL026051.

Sokolik I., and O. Toon, 1999: Incorporation of mineralogical composition into models of the radiative properties of mineral aerosol from UV to IR wavelengths. *J. Geophys. Res.* **104**:9423-9444, doi:10.1029/1998JD200048.

Sokolik I., D. Winker, G. Bergametti, et al., 2001: Introduction to special section: outstanding problems in quantifying the radiative impacts of mineral dust. *J. Geophys. Res.* **106**:18015-18027.

Solomon P. A., W. Chameides, R. Weber, A. Middlebrook, C. S. Kiang, A. G. Russell, A. Butler, B. Turpin, D. Mikel, R. Scheffe, E. Cowling, E. Edgerton, J. St. John, J. Jansen, P. McMurry, S. Hering, and T. Bahadori, 2003: Overview of the 1999 Atlanta Supersite Project. *J. Geophys. Res.* **108(D7):**8413, doi:10.1029/2001JD001458

Spinhirne J., S. Palm, W. Hart, D. Hlavka, and E. Welton, 2005: Cloud and Aerosol Measurements from the GLAS Space Borne Lidar: initial results. *Geophys. Res. Let.* **32**:L22S03, doi:10.1029/2005GL023507.

Stanhill G., and S. Cohen, 2001: Global dimming: a review of the evidence for a widespread and significant reduction in global radiation with discussion of its probable causes and possible agricultural consequences. *Agricul. Forest Meteorol.* **107**:255-278.

Stephens G., R. Engelen, M. Vaughan, and T. Anderson: Toward retrieving properties of the tenuous atmosphere using space-based lidar measurements. *J. Geophys. Res.* **106**:28143-28157.

Stephens G., D. Vane, R. Boain, G. Mace, K. Sassen, Z. Wang, A. Illingworth, E. O'Conner, W. Rossow, S. Durden, S. Miller, R. Austin, A. Benedetti, and C. Mitrescu, 2002: The CloudSat mission and the A-Train. *Bull. Amer. Meteo. Soc.* **83**:1771-1790.

Stier P., J. Seinfeld, S. Kinne, J. Feichter, and O. Boucher, 2006: Impact of nonabsorbing anthropogenic aerosols on clear-sky atmsopheric absorption. *J. Geophys. Res.* **111**:D18201, doi:10.1029/2006JD007147.

Strawa A., R. Castaneda, T. Owano, P. Baer, and B. Paldus, 2002: The measurement of aerosol optical properties using continuous wave cavity ring-down techniques. *J. Atm. Ocean. Tech.* **20**:454-465.

Streets D., and K. Aunan, 2005: The importance of China's household sector for black carbon emissions. *Geophys. Res. Lett.* **32**:L12708, doi:10.1029/2005GL022960.

Streets D., T. Bond, T. Lee, and C. Jang, 2004: On the future of carbonaceous aerosol emissions. *J. Geophys. Res.* **109**:D24212, doi:10.1029/2004JD004902.

Streets D., Q. Zhang, L. Wang, K. He, J. Hao, Y. Tang, and G. Carmichael, 2006a: Revisiting China's CO emissions after TRACE-P: Synthesis of inventories, atmospheric modeling and observations *J. Geophys. Res.* **111:**D14306, doi:10.1029/2006JD007118.

Streets D., Y. Wu, and M. Chin, 2006b: Two-decadal aerosol trends as a likely explanation of the global dimming/brightening transition. *Geophys. Res. Lett.* **33**:L15806, doi:10.1029/2006GL026471.

Takemura T., H. Okamoto, Y. Maruyama, A. Numaguti, A. Higurashi, and T. Nakajima, 2000: Global three-dimensional simulation of aerosol optical thickness distribution of various origins. *J. Geophys. Res.* **105**:17853-17873.

Takemura T., T. Nakajima, O. Dubovik, B. Holben, and S. Kinne, 2002: Single-scattering albedo and radiative forcing of various aerosol species with a global three-dimensional model. *J. Climate*, **15**:333-352.

Takemura, T., T. Nozawa,S. Emori, T. Nakajima, and T. Nakajima, 2005: Simulation of climate response to aerosol direct and indirect effects with aerosol transport-radiation model. *J. Geophys. Res.* **110**:D02202, doi:10.1029/2004JD005029.

Tang Y., G. Carmichael, I. Uno, J. Woo, G. Kurata, B. Lefer, R. Shetter, H. Huang, B. Anderson, M. Avery, A. Clarke and D. Blake, 2003: Influences of biomass burning during the Transport and Chemical Evolution Over the Pacific (TRACE-P) experiment identified by the regional chemical transport model. *J. Geophys. Res.* **108:**8824, doi:10.1029/2002JD003110.

Tang Y., G. Carmichael, J. Seinfeld, D. Dabdub, R. Weber, B. Huebert, A. Clarke, S. Guazzotti, D. Sodeman, K. Prather, I. Uno, J. Woo, D. Streets, P. Quinn, J. Johnson, C. Song, A. Sandu**,** R. Talbot and J. Dibb, 2004: Three-dimensional simulations of inorganic aerosol distributions in East Asia during spring 2001. *J. Geophys. Res.* **109**:D19S23, doi:10.1029/2003JD004201.

Tanré D., Y. Kaufman, M. Herman, and S. Mattoo, 1997: Remote sensing of aerosol properties over oceans using the MODIS/EOS spectral radiances. *J. Geophys. Res.*, **102**:16971-16988.

Tanré D., J. Haywood, J. Pelon, J. Léon, B. Chatenet, P. Formenti, P. Francis, P. Goloub, E. Highwood, and G. Myhre, 2003: Measurement and modeling of the Saharan dust radiative impact: Overview of the Saharan Dust Experiment (SHADE). *J. Geophys. Res.* **108**:8574, doi:10.1029/2002JD003273.

Tegen I., and I. Fung, 1995: Contribution to the atmospheric mineral aerosol load from land surface modification. *J. Geophys. Res.* **100**:18707-17726.

Tegen I., M. Werner, S. Harrison, and K. Kohfeld, 2004: Relative importance of climate and land use in determining present and future global soil dust emission. *Geophy. Res. Lett.* **31**:L05105, doi:10.1029/2003GL019216.

Textor C., M. Schulz, S. Guibert, et al., 2006: Analysis and quantification of the diversities of aerosol life cycles within AEROCOM. *Atmos. Chem. Phys.* **6**:1777-1813.

Torres O., P. Bhartia, J. Herman, Z. Ahmad, and J. Gleason, 1998: Derivation of aerosol properties from satellite measurements of backscattered ultraviolet radiation: Theoretical bases. *J. Geophys. Res.* **103**:17009-17110.

Torres O., P. Bhartia, J. Herman, A. Sinyuk, P. Ginoux, and B. Holben, 2002: A long-term record of aerosol optical depth from TOMS observations and comparison to AERONET measurements. *J. Atmos. Sci.* **59**:398--413.

Torres O., P. Bhartia, A. Sinyuk, E. Welton, and B. Holben, 2005: Total Ozone Mapping Spectrometer measurements of aerosol absorption from space: Comparison to SAFARI 2000 ground-based observations. *J. Geophys. Res.* **110**:D10S18, doi:10.1029/2004JD004611.

Tsvetsinskaya E., C. Schaaf, F. Gao, et al., 2002: Relating MODIS-derived surface albedo to soils and rock types over Northern Africa and the Arabian Peninsula. *Geophys. Res. Lett.* **29**:1353, doi:10.1029/2001GL014096.

Twomey S., 1977: The influence of pollution on the shortwave albedo of clouds. *J. Atmos. Sci.* **34**:1149-1152.

Wang J., S. Christopher, F. Brechtel, J. Kim, B. Schmid, J. Redemann, P. Russell, P. Quinn, and B. Holben, 2003: Geostationary satellite retrievals of aerosol optical thickness during ACE-Asia. *J. Geophys. Res.* **108**:8657, 10.1029/2003JD003580.

Welton E., K. Voss, P. Quinn, P. Flatau, K. Markowicz, J. Campbell, J. Spinhirne, H. Gordon, and J. Johnson, 2002: Measurements of aerosol vertical profiles and optical properties during INDOEX 1999 using micro-pulse lidars. *J. Geophys. Res.* **107**:8019, doi:10.1029/2000JD000038.

Welton E., J. Campbell, J. Spinhirne, and V. Scott, 2001: Global monitoring of clouds and aerosols using a network of micro-pulse lidar systems, in *Lidar Remote Sensing for Industry and Environmental Monitoring*, U. N. Singh, T. Itabe, N. Sugimoto, (eds.), *Proc. SPIE*, **4153**:151-158.

Wen G., A. Marshak, and R. Cahalan, 2006: Impact of 3D clouds on clear sky reflectance and aerosol retrieval in a biomass burning region of Brazil. *IEEE Geo. Rem. Sens. Lett.* **3**:169-172.

Wetzel, M. A. and Stowe, L. L.: Satellite-observed patterns in stratus microphysics, aerosol optical thickness, and shortwave radiative forcing. 1999: *J. Geophys. Res.*, **104**:31287-31299.

Wielicki B., B. Barkstrom, E. Harrison, R. Lee, G. Smith, and J. Cooper, 1996: Clouds and the Earth's radiant energy system (CERES): An Earth observing system experiment. *Bull. Amer. Meteo. Soc.* **77**:853-868.

Wild M., H. Gilgen, A. Roesch, et al., 2005: From dimming to brightening: Decadal changes in solar radiation at Earth's surface. *Science* **308**:847-850.

Winker D., J. Pelon, and M. McCormick, 2003: The CALIPSO mission: spaceborne lidar for observation of aerosols and clouds. *Proc. SPIE* **4893**:1-11.

Yu H., S. Liu, and R. Dickinson, 2002: Radiative effects of aerosols on the evolution of the atmospheric boundary layer. *J. Geophys. Res.* **107:**4142, doi:10.1029/2001JD000754.

Yu H., R. Dickinson, M. Chin, Y. Kaufman, B. Holben, I. Geogdzhayev, and M. Mishchenko, 2003: Annual cycle of global distributions of aerosol optical depth from integration of MODIS retrievals and GOCART model simulations. *J. Geophys. Res.* **108**:4128, doi:10.1029/2002JD002717.

Yu H., R. Dickinson, M. Chin, Y. Kaufman, M. Zhou, L. Zhou, Y. Tian, O. Dubovik, and B. Holben, 2004: The direct radiative effect of aerosols as determined from a combination of MODIS retrievals and GOCART simulations. *J. Geophys. Res.* **109**:D03206, doi:10.1029/2003JD003914.

Yu H., Y. Kaufman, M. Chin, G. Feingold, L. Remer, T. Anderson, Y. Balkanski, N. Bellouin, O. Boucher, S. Christopher, P. DeCola, R. Kahn, D. Koch, N. Loeb, M. S. Reddy, M. Schulz, T. Take-

mura, and M. Zhou, 2006: A review of measurement-based assessments of aerosol direct radiative effect and forcing. *Atmos. Chem . Phys.* **6**:613-666.

Yu H., R. Fu, R. Dickinson, Y. Zhang, M. Chen, and H. Wang, 2007: Interannual variability of smoke and warm cloud relationships in the Amazon as inferred from MODIS retrievals. *Remote Sens. Environ.* **111**:435-449.

Zhang J., and S. Christopher, 2003: Longwave radiative forcing of Saharan dust aerosols estimated from MODIS, MISR, and CERES observations on Terra. *Geophys. Res. Lett.* **30**:2188, doi:10.1029/2003GL018479.

Zhang J., S. Christopher, L. Remer, and Y. Kaufman, 2005a: Shortwave aerosol radiative forcing over cloud-free oceans from Terra. I: Angular models for aerosols. *J. Geophys. Res.* **110**:D10S23, doi:10.1029/2004JD005008.

Zhang J., S. Christopher, L. Remer, and Y. Kaufman, 2005b: Shortwave aerosol radiative forcing over cloud-free oceans from Terra. II: Seasonal and global distributions. *J. Geophys. Res.* **110**:D10S24, doi:10.1029/2004JD005009.

Zhang Q., C.O. Stanier, M.R. Canagaratna, J.T. Jayne, D.R. Worsnop, S.N. Pandis, and J.L. Jimenez, 2004; Insights into the chemistry of new particle formation and growth events in Pittsburgh based on aerosol mass spectrometry. Environ. Sci. Technol. 38(18):4797 -4809, 10.1021/es035417u S0013-936X(03)05417-8.

Zhao T. X.-P., H. Yu, I. Laszlo, M. Chin, and W.C. Conant, 2008: Derivation of component aerosol direct radiative forcing at the top of atmosphere for clear-sky oceans. *J. Quant. Spectro. Rad. Trans.* **109:**1162-1186.

Zhou M., H. Yu, R. Dickinson, O. Dubovik, and B. Holben, 2005: A normalized description of the direct effect of key aerosol types on solar radiation as estimated from AERONET aerosols and MODIS albedos. *J. Geophys. Res.* **110**:D19202, doi:10.1029/2005JD005909.

Acronyms and Symbols

ABC	Asian Brown Cloud
ACE	Aerosol Characterization Experiment
AD-Net	Asian Dust Network
ADEOS	Advanced Earth Observation Satellite
ADM	Angular Dependence Models
AeroCom	Aerosol model and observation intercomparison project
AERONET	Aerosol Robotic Network
AI	Aerosol Index
AIOP	Aerosol Intensive Operative Period
AOD (τ)	Aerosol optical depth
APS	Aerosol Polarimetry Sensor
AR4	IPCC Forth Assessment Report
ARM	Atmospheric Radiation Measurements
AVHRR	Advanced Very High Resolution Radiometer
A-Train	Constellation of six afternoon overpass satellites
BASE-A	Biomass Burning Airborne and Spaceborne Experiment Amazon and Brazil
BRDF	Bidirectional Reflectance Distribution Function
CALIOP	Cloud and Aerosol Lidar with Orthogonal Polarization

CALIPSO	Cloud Aerosol Infrared Pathfinder Satellite Observations
CCN	Cloud Condensation Nuclei
CCRI	Climate Change Research Initiative
CCSP	Climate Change Science Program
CERES	Clouds and the Earth's Radiant Energy System
CLAMS	Chesapeake Lighthouse and Aircraft Measurements for Satellite campaign
CTM	Chemical Transport Model
DAAC	Distributed Active Archive Center
DCF	Direct climate forcing (anthropogenic aerosols)
DRE	Direct radiative effect (total aerosols)
EARLINET	European Aerosol Research Lidar Network
EAST-AIRE	East Asian Studies of Tropospheric Aerosols: An International Regional Experiment
EOS	Earth Observing System
ERBE	Earth Radiation Budget Experiment
Eτ	Radiative Efficiency (aerosol radiative effect normalized by AOD)
GCM	General Circulation Model
GEOS	Goddard Earth Observing System
GFDL	Geophysical Fluid Dynamics Laboratory (NOAA)
GHGs	Greenhouse Gases
GISS	Goddard Institute for Space Studies (NASA)
GLAS	Geoscience Laser Altimeter System
GMD	Global Modeling Division (NOAA)
GMI	Global Modeling Initiative
GOCART	Goddard Chemistry Aerosol Radiation and Transport
GOES	Geostationary Operational Environmental Satellite
GSFC	Goddard Space Flight Center (NASA)
ICARTT	International Consortium for Atmospheric Research on Transport and Transformation
ICESat	Ice, Cloud, and Land Elevation Satellite
IMPROVE	Interagency Monitoring of Protected Visual Environment
INCA	Interactions between Chemistry and Aerosol (LMDz model)
INDOEX	Indian Ocean Experiment
INTEX-NA	Intercontinental Transport Experiment – North America
IPCC	Intergovermental Panel on Climate Change
IR	Infrared radiation
LBA	Large-Scale Biosphere-Atmosphere Experiment in Amazon
LMDZ	Laboratoire de Météorologie Dynamique with Zoom
LOA	Laboratoire d' Optique Atmosphérique
LOSU	Level of Scientific Understanding
LWP	Liquid Water Path
MAN	Maritime Aerosol Network
MFRSR	Multifilter Rotating Shadowband Radiometer
MINOS	Mediterranean Intensive Oxidant Study
MISR	Multi-angle Imaging SpectroRadiometer
MODIS	Moderate Resolution Imaging Spectroradiometer
MPLNET	Micro Pulse Lidar Network

NASA	National Aeronautics and Space Administration
NEAQS	New England Air Quality Study
NOAA	National Oceanography and Atmosphere Administration
NPOESS	National Polar-orbiting Operational Environmental Satellite System
NPP	NPOESS Preparatory Project
OMI	Ozone Monitoring Instrument
PARASOL	Polarization and Anisotropy of Reflectance for Atmospheric Science coupled with Observations from a Lidar
PEM-West	Western Pacific Exploratory Mission
POLDER	Polarization and Directionality of the Earth's Reflectance
POM	Particulate Organic Matter
PRIDE	Pueto Rico Dust Experiment
REALM	Regional East Atmospheric Lidar Mesonet
RH	Relative Humidity
RTM	Radiative Transfer Model
SAFARI	South Africa Regional Science Experiment
SCAR-A	Smoke, Clouds, and Radiation – America
SCAR-B	Smoke, Clouds, and Radiation - Brazil
SeaWiFS	Sea-viewing Wide Field-of-view Sensor
SHADE	Saharan Dust Experiment
SMOCC	Smoke, Aerosols, Clouds, Rainfall and Climate
SPRINTARS	Spectral Radiation-Transport Model for Aerosol Species
SSA (ω_0)	Aerosol Single-Scattering Albedo
STEM	Sulfate Transport and Deposition Model
TAR	IPCC Third Assessment Report
TARFOX	Tropospheric Aerosol Radiative Forcing Observational Experiment
TOA	Top-Of-Atmosphere
TOMS	Total Ozone Mapping Spectrometer
TRACE-A	Transport and Chemical Evolution over the Atlantic
TRACE-P	Transport and Chemical Evolution over the Pacific
UAE^2	United Arab Emirates Unified Aerosol Experiment
UV	Ultraviolet radiation